POLITECNICO
MILANO 1863

DIPARTIMENTO DI
INGEGNERIA CIVILE E AMBIENTALE

Non-Planar Reinforced Concrete Walls: Review of Literature and Finite Element Modeling with OpenSees

TESI DI LAUREA MAGISTRALE IN
CIVIL ENGINEERING
INGEGNERIA CIVILE e AMBIENTALE

Author: **Shady Emad Nabih Hefzy**

Student ID: 10816970
Advisor: Prof. Federico Perotti
Co-advisor: Prof. Luca Martinelli
Academic Year: 2022-2023

Acknowledgments

I would like to express my sincere gratitude to all who have contributed to the completion of this master's thesis. My extreme appreciation goes to my advisors, Prof. Federico Perotti and Prof. Luca Martinelli for their mentorship, guidance, expertise, and their commitment throughout this research journey. Their continuous positive feedback has made the development of the thesis very significant.

Thanks should also go to the school and the staff of the Civil, Environmental and Land Management Engineering whose academic resources and research facilities have been the base for this research.

Boundless appreciation should go for professor K. Beyer and professor R. Constantin for suppling full experimental data which was a great help building this research. Moreover, Sincere thanks goes to professor Kolozvari for his support during the modeling by MVLEM-3D element.

Appreciative recognition should be dedicated to "ASDEA Software Technology" for developing STKO software which allowed a better visualization of building the model in OpenSees and easier post processing of the results.

A heartfelt acknowledgement to my family, friends and specially my life partner Monica for their support, patience and understanding during the whole period of research. Their motivation and belief in my abilities have been the force that pushes me to give more and more.

Finally, I am grateful to all the individuals who contributed their time or efforts, without whom this study would not have been possible.

Abstract

In recent engineering practice, non-planar walls have become dominant as structural elements. However, they are commonly used, there exists a limited number of comprehensive research and experimental tests clarifying the inelastic behavior of non-planar walls subjected to different seismic loading directions. This thesis focuses on enhancing the modeling techniques and the design for non-planar walls by creating and validating a numerical model through finite element analysis with OpenSees. A 3-D analytical model of the non-planar wall was developed in OpenSees using MVLEM3-D element. Then the model is validated by the experimental results of the test units that were tested under a certain loading protocol which was multidirectional one. The model successfully captured the global response "load-deformation" and local response "strains". By comparing the experimental and numerical model results, it was determined that the model with MVLEM3-D element was able to capture the cyclic load-displacement behavior of the non-planar wall when loaded in the direction of the principal axes with good accuracy. However, when loaded in the diagonal direction, the model overestimated the strength of the wall by approximately 50%. This is attributed to the plane section hypotheses maintained in the MVLEM 3-D element formulation that was insufficient to capture all the observed complex failure mechanisms that led to loss of the load carrying capacity and the strain distributions across the wall due to the shear lag effect.

Keywords: non-planar walls; quasi-static cyclic Test; multi-directional loading; hysteretic behavior; finite element modeling; opensees; distributed plasticity; flexural dominated response.

Abstract in Italiano

Nella recente pratica ingegneristica, le pareti non piane sono diventate predominanti come elementi strutturali. Tuttavia, sebbene vengano comunemente impiegate, esiste un numero limitato di ricerche esaustive e test sperimentali che chiariscano il comportamento inelastico delle pareti non piane sottoposte a diverse direzioni di carico sismico. Questa tesi si concentra sul miglioramento delle tecniche di modellazione e progettazione per le pareti non piane mediante la creazione e la validazione di un modello numerico mediante analisi agli elementi finiti con OpenSees. Un modello analitico tridimensionale della parete non piana è stato sviluppato in OpenSees utilizzando l'elemento MVLEM3-D. Successivamente, il modello è stato validato attraverso i risultati sperimentali delle unità di prova testate secondo un determinato protocollo di carico multidirezionale. Il modello ha efficacemente catturato la risposta globale "carico-deformazione" e la risposta locale in termini di deformazioni. Confrontando i risultati del modello sperimentale e numerico, è emerso che il modelo è stato in grado di riprodurre con precisione il comportamento ciclico carico-spostamento della parete non piana quando caricata nella direzione degli assi principali. Tuttavia, quando caricato nella direzione diagonale, il modello ha sovrastimato la resistenza della parete di circa il 50%. Questo è attribuito alle ipotesi di sezione piana mantenute nella formulazione dell'elemento MVLEM 3-D, che si sono rivelate insufficienti per catturare tutti i complessi meccanismi di rottura osservati che hanno portato alla perdita della capacità portante del carico e alla distribuzione delle deformazioni lungo la parete a causa dell'effetto di ritardo al taglio.

Parole chiave: pareti non piane; Test ciclico quasi-statico; carico multidirezionale; comportamento isteretico; modellazione agli elementi finiti; opensees; plasticità distribuita; risposta dominata dalla flessione.

List of Contents

List of Figures

List of Tables

List of Symbols

Variable	Description	SI unit
f_c	Compressive strength of concrete	MPa
A_g	Gross section area	mm^2
μ	Ductility level	-
Δ_f	Flexural displacement	mm
Δ_s	Shear displacement	mm
$\Delta_{p,f}$	Plastic flexural displacement	mm
Δ_y	Nominal yield displacement	mm
Φ_y	Nominal yield curvature of a wall section	-
Φ'_y	First yield curvature of a wall section	-

1 Introduction

1.1. Background and Motivation

In the field of reinforced concrete (RC) building design, the structural integrity of high-rise constructions heavily relies on the core, a fundamental element capable of accommodating features like lift shafts and stairs. Cores possess a characteristic cellular section, usually enclosed on three sides, with the fourth side either open or partially closed by strong coupling beams (Figure 1.2). Although the basic U-shaped or channel section is frequent, complex multicellular shapes (Figure 1.1) are increasingly common in current high-rise structures. While simpler wall shape designs are known to be predictable in their inelastic cyclic behavior, the unusual behavior of cores with complex shapes remains challenging to be captured with the necessary accuracy, which leads to nearly elastic approach in their design.

Figure 1.1 Cross Sections of non-planar walls

In recent years, considerable research has been developed into the seismic response of RC walls with rectangular cross-sections. Numerous experimental studies and tests have resulted in the effective parameters governing the behavior of these walls under seismic excitation. These findings have been integrated into code provisions, offering bold guidelines for engineers designing rectangular walls. However, despite the widespread use of core walls in practical applications, their inelastic behavior under seismic loads remains unknown. Limited number of experiments, mainly focused on U-shaped walls under cyclic loading have been carried out in the past, leaving a gap in experimental evidence. This few numbers of experiments hampers the adequate

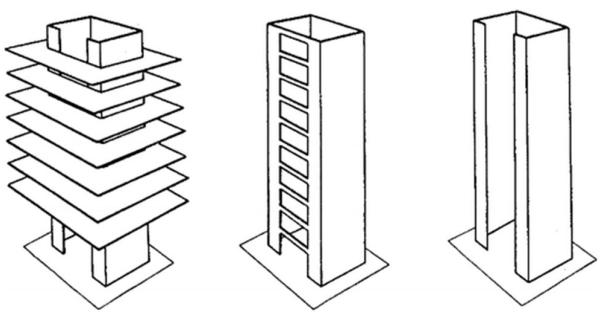

Figure 1.2 Open and partially closed core

calibration of analytical models and the derivation of applicable design standards, making it harder to fill this knowledge gap.

In contrast to the rectangular walls, which solely resist lateral forces in one direction, core structures provide lateral stiffness and strength in both horizontal directions and diagonally. This distinctive characteristic highlights the vital role played by core structures in ensuring not only the strength but also displacement demands in the face of complex seismic loading paths, highlighting their significance in modern building design standards.

1.2. Problem Statement

When designing the structural scheme of an RC building having a core structure, engineers encounter two major challenges. The obstacle revolves around how to accurately model these complex non-planar wall configurations and obtain accurate approximations of their behavior concerning both displacements and capacity demands. This requires sophisticated modeling techniques to envelope the complexity of core structures and ensure a reliable representation of their responses in real-world situations.

1.3. Objectives and scope of the study

The overall goals of this study are focusing on improving the design and modeling processes for RC buildings containing core structures. In a more specific view, the study aims to deepen our sight of the inelastic behavior displayed by cores when subjected to different seismic loading directions. By focusing on these specific objectives, the research aims to enhance the field's knowledge and promote more precise and effective design approaches for buildings with core elements.

The scope of this study is focused on U-shaped walls, which, despite their clear simplicity, display complexities in both elastic and inelastic behavior exceeding those of rectangular walls. This specific core shape is composed of multiple interconnected rectangular sections, leaving one side left open, providing flexural resistance in both horizontal directions as well as torsional stiffness. Within the seismic design context of U-shaped walls, this study aims to accomplish the following objective:

- Develop and validate direct numerical models available to engineers for the analysis of the behavior of non-planar walls.

1.4. Outline of report

The report is divided into six chapters. The initial chapter is an introductory one. This chapter discusses the different challenges and problems that are faced in the modeling of non-planar shear walls. Then, it states the main objective of this thesis. Chapter two

refers to the comprehensive review of literature of the non-planar walls and different modeling approaches. While Chapter three goes into detail in one of the non-planar walls "U-shaped wall" experimental test and description of the failure mechanisms and hysteretic behavior under multi-directional loading protocol. Chapter four is specially devoted to modeling of the non-planar test units by using the software OpenSees. Chapter five is a verification of the experimental results with the numerical model results. Finally, Chapter six is a summary and presents the conclusion to the whole thesis with addition to a recommendation for future work.

More in details:

Chapter two gives a brief literature review on the different testing of non-planar walls under different loading protocols with some conclusions on the behavior of the walls and on the damage process that led to failure and how this failure could be prevented. So, it highlights the main parameters that affect the behavior of the walls. Also, it reviews different modeling approaches of the numerical models for the non-planar walls.

In Chapter three, a further discussion is presented of the quasi-static cyclic tests done on three test units of U-shaped walls, presented in chapter two, in terms of test set up, the loading history and the experimental results during the tests. The walls were tested under bi-directional loading protocol that was defined in a more refined way in addition to the constant axial load applied at the top of the test units. The geometry and detailing of the reinforcement layout of the three test units are described precisely. The damage procedure is stated in detail till reaching the total loss of the load carrying capacity of each wall.

Chapter four states in details the modeling process of the three test units using the analysis software OpenSees. A displacement-control test is applied on the three test units. The walls are modelled using the MVLEM3-D element that has a good accuracy in capturing the behavior of the walls both from a global response "load-deformation" point of view and local response "strains". A definition of each of concrete and steel constitutive laws and its implementation in the OpenSees is provided and the parameters used are given. The discretization of each wall segment into number of fibers is shown with the ratio of reinforcement steel according to this division. In addition the solver technique used is presented.

In Chapter five, the experimental results are compared with the numerical results from the model in chapter four. The results show that the MVLEM3-D element is able to capture the cyclic load-displacement behavior of the non-planar walls when loaded parallel to the principal directions of the cross section with good accuracy. While loading in a diagonal direction, it overestimates the wall strength with an average of 50% higher than the experimental test results. The plane section hypotheses implemented in the formulation of the MVLEM3-D element is the reason behind this

overestimation which makes the model unable to capture all the observed non-linear strain distribution along the wall through the experiment.

In the final chapter the main output of the research is summarized and is concluded with suggestions to further research needs concerning the behavior of the non-planar walls under bi-directional loading.

2 Literature Review

2.1. Review of non-planar composite shear walls testing under quasi-static cyclic Loading

2.1.1. (Ile & Reynouard, 2005) ,(Reynouard & Fardis, 2001) and(Pégon et al., 2000): U-shaped Wall Tests

Reynouard and Fardis (2001) carried out the overall design and analysis of three U-Shaped walls, which were latterly tested under quasi-static cyclic loading at the European Laboratory for Structural Assessment (ELSA) by Pegón et al. (2000). The study focused on the enhancement of understanding the nonplanar walls' seismic response, upgrading the numerical modeling techniques for nonplanar walls under combined loading, and proposed practical design recommendations. The U-Shaped walls shared identical cross-section geometry (Figure 2.1) and reinforcement layout, and were designed in conformity with(EN 1998-1, 1998).

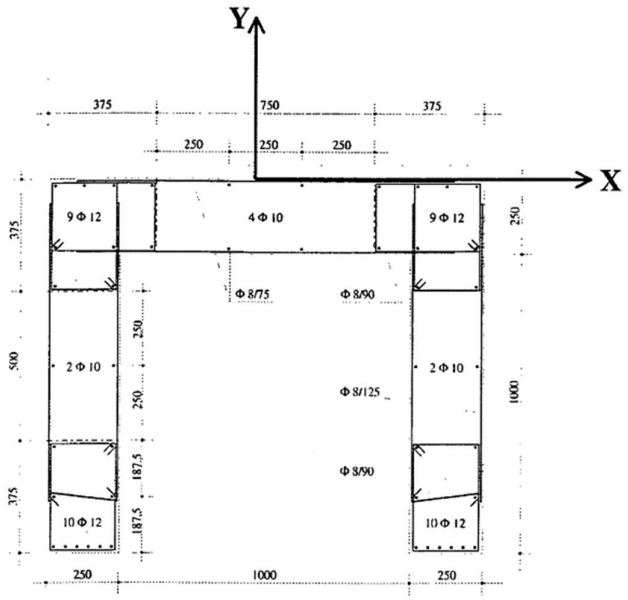

Figure 2.1 Cross Section of Ispra test specimen scale 1:1.
Dimensions in mm. (Ile & Reynouard, 2005)

The three wall samples experienced varying lateral displacement patterns (Figure 2.2). In the initial two tests, the walls faced cyclic lateral loading in a single direction: Wall 1 was pushed in the X-direction (aligned with the wall's web, inducing bending in strong axis), Wall 2 was pushed loading in the Y-direction (perpendicular to the wall's web, inducing bending in weak axis), and wall 3 was subjected to a square clover leaf pattern, so that a diagonal loading could be achieved leading to both X and Y displacement components which helped studying the bi-directional loading behavior of the wall. In which the pattern was in a sequence of O→D→F→B→A→E→C→O and O→D→G→A→B→H→C→O.

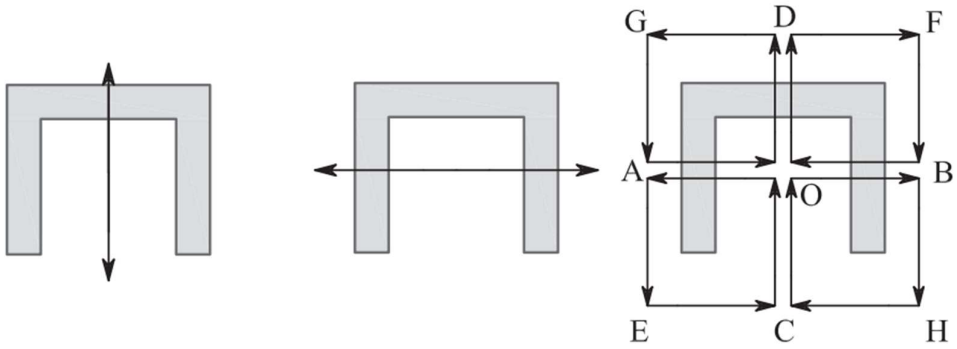

(a) Wall 1 (b) Wall 2 (c) Wall 3

Figure 2.2 Loading Paths for Ispra Tests (Ile & Reynouard, 2005)

The experimental test program showed significant insights. It was noticed that bi-directional loading led to decreasing drift capacity in both strong and weak axis loading directions and led to much strength degradation compared to unidirectional loading. Researchers also observed that under bidirectional loading, shear forces in the Y-direction (bending weak axis) were mainly resisted by the flange that is under compression, while the flange that was subjected to tension only carried a limited portion of the shear force in the flanges' direction. Therefore, the study recommended designing each flange of the two wall flanges to resist the entire shear force applied in the direction of the wall flanges. Lastly, the researchers also pointed out the sufficiency of critical region confinement as stated in EN1998-1:2001.

Figure 2.3 Shear failure of one flange end in Ispra Test(Ile & Reynouard, 2005)

2.1.2. (Beyer et al., 2008b) : U-shaped Wall Test

At ETH Zurich, two U-shaped walls (TUA and TUB) were tested to extend the research carried out by Ile and Reynouard (2005). This study aimed to elevate the understanding of many key aspects of the U-shaped shear walls: i) The U-shaped walls sensitivity to shear and sliding shear mechanisms, ii) The load direction impact on deformation, stiffness, and strength capacity, iii) The participation of shear, sliding, and flexural deformations to the overall deformation of the walls.

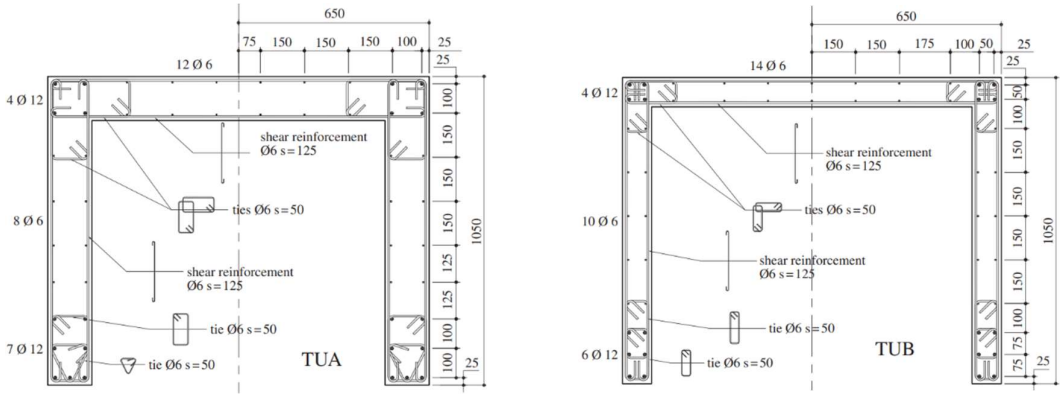

(a)TUA (b)TUB

Figure 2.4 Cross section of the test specimen by (Beyer et al., 2008b) scale 1:2. Dimensions in mm.

The principal variable under investigation was wall thickness, as it was predicted to greatly affect the shear response mechanisms previously witnessed by Ile and Reynouard (2005). The specimens were not specifically designed to comply with any specific design code. Instead, they were thoroughly detailed to achieve high ductility demands without excessively conservative with respect to estimates of shear and sliding shear strength. Both specimens were provided with concrete shear keys at the wall-foundation interface to overcome sliding shear forces. The walls were subjected to a loading scenario, consisting of a cruciform clover leaf pattern (Figure 2.5) stimulating independent bending in the strong and weak axis, a diagonal load cycle stimulating bending in the strong and weak axis, and a bi-directional "sweep" stimulating strong- and weak-axis bending at increasing levels of ductility demand. Moreover, a constant axial load was applied to each specimen, corresponding to $0.02.f'_c.A_g$ for TUA and $0.04.f'_c.A_g$ for TUB. This setup allowed for a in depth understanding of the structural behavior under different conditions.

The loading directions are:

For a full EW cycle in direction parallel to the web: O→A→B→O

For a full NS cycle in direction parallel to the flanges: O→C→D→O

For a full Diagonal cycle: O→E→F→O

For the sweep: O→A→G→D→C→H→B→O

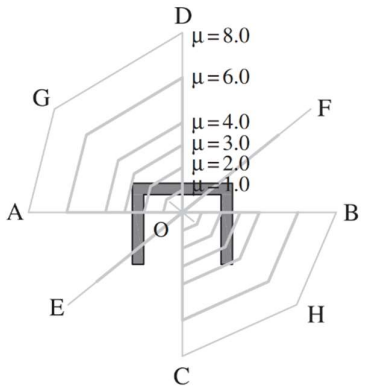

Figure 2.5 Loading Paths for TUA and TUB

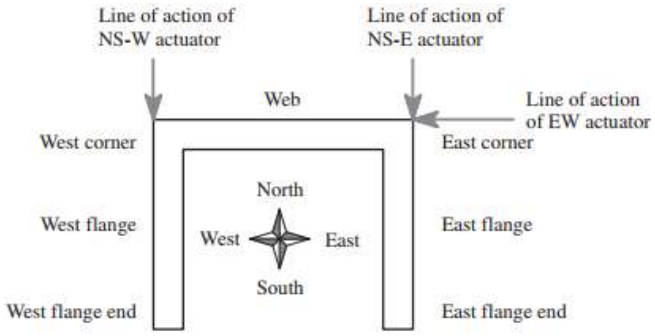

Figure 2.6 Labelling of different wall sections

The output of the tests highlighted several crucial aspects in the behavior of non-planar walls. However, in spite the efforts made to ensure ductile response during the design of the test specimens, the thinner wall TUA failed due to compression. This phenomenon was linked to intense spalling of the concrete boundary element when subjected to bidirectional loading. Consequently, this led to a great reduction in cross-sectional area and compressive load carrying capacity. Furthermore, TUB failed due to the crushing of the unconfined web zone. This finding is significant, especially given that current design and analysis software often misses to capture the wall response under bi-directional loading due to the limitations of the plane section hypothesis. Additionally, the study observed that shear deformation in non-planar walls changes based on the direction of loading and can greatly overtake the levels observed in planar walls. This variation indicates that unique provisions may be needed for the design of non-planar walls to consider these distinctive behaviors. The failure of TUA and TUB are presented in Figure 2.7 and Figure 2.8 respectively.

(a) (b)

Figure 2.7 Failure of TUA (Beyer et al., 2008b)

a)Rupture of boundary element longitudinal bars in the west flange, and b)overall cracking pattern and crushing in TUA

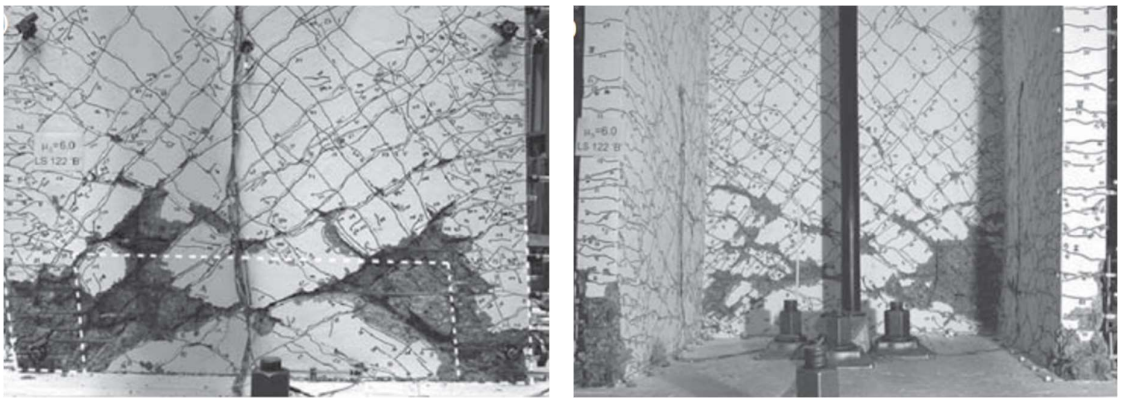

(a) (b)

Figure 2.8 Failure of TUB (Beyer et al., 2008b)

a)Crushing of unconfined zones in the web, and b)overall cracking pattern and crushing in TUB

2.1.3. (Lowes et al., 2014) : C-shaped Wall Test

Three alike C-shaped walls were investigated within a coordinated research effort between the University of Washington and the University of Illinois at Urbana-Champaign. These tests were based on assessing the earthquake performance of slender walls that comply with modern ACI Code standards. The main goal of this research was to construct guidelines for the performance-based seismic design of reinforced concrete walls with irregular geometries. In pursuit of this goal, a combination of experimental testing and numerical modeling was developed to

understand non-planar wall behavior, therefore enriching the understanding of wall design principles.

The C-shaped wall test specimens represented the lower three stories of a 10-story prototype building, with 1:3 scale models. The design of these wall specimens was done relying on data obtained from a building inventory on the West Coast and with the help of external advisory panel, who were a group of structural engineers from "Magnusson Klemencic Associates." The design of the specimens was strictly following the guidelines outlined in (ACI 318-05, 2005) and (ASCE-7, 2006). The name "C-shaped" was specifically chosen to describe these specimens due to large variation between the length of the flanges in comparison to the web (flange to web ratio of 0.4). The three specimens had the same geometry, materials, boundary conditions, and reinforcement. The boundary elements of the specimens were heavily reinforced with longitudinal reinforcement located at the flange ends and wall corners, while the interior regions between these boundary elements, were lightly reinforced in the vertical and horizontal directions.

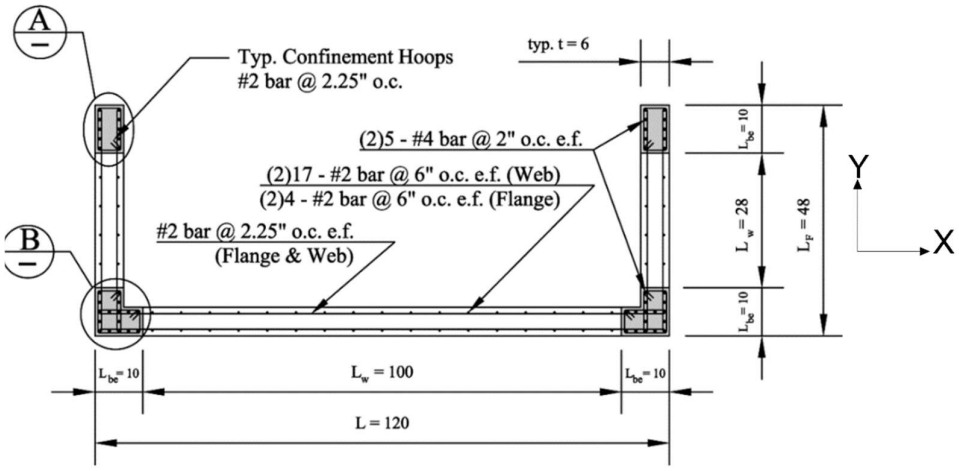

Figure 2.9 Cross section of the test specimen CW1,CW2,CW3 scale 1:3.
Dimensions in inches. (Lowes et al., 2014)

The loading conditions were the only variation between the three walls CW1, CW2 and CW3. The loading paths are defined in Figure 2.10. For CW1, it was laterally loaded in unidirectional cyclic in the X-direction (parallel to the web, inducing bending in strong axis) with a constant axial load of $0.05f'_c.A_g$. For CW2, it was loaded laterally in a bidirectional loading -pattern in both the X- and Y-directions (parallel and perpendicular to the web, inducing bending in both strong and weak axes) with the same constant axial load. The maximum drift capacity of the loading apparatus was attained without observing any strength loss. For CW3, it was loaded in a way to simulate the loading conditions of a coupled wall system. This particular specimen was subjected to a cruciform lateral displacement history. The axial load remained constant at $0.05f'_c.A_g$ for loading in the X-direction (strong axis), while the axial load

alternated between tension and compression in the Y-direction (weak axis) to take into consideration the effect of the coupling beams.

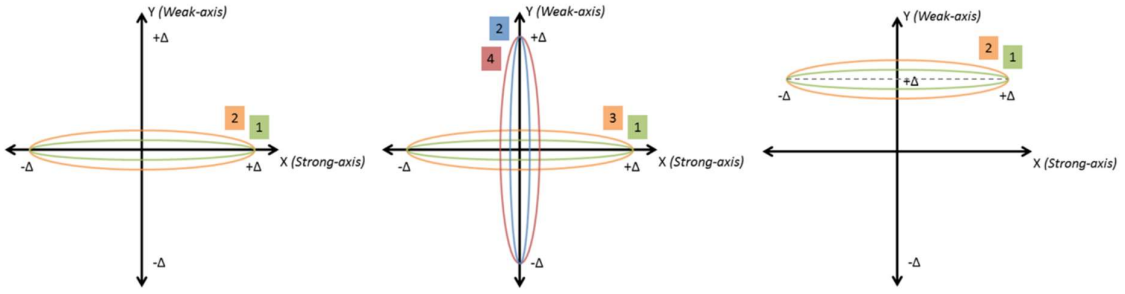

(a) CW1 (b) CW2 (c) CW3

Figure 2.10 Loading path (Lowes et al., 2014)

For all the three specimens, buckling-rupture of longitudinal bars was the reason behind the loss of lateral load-carrying capacity. Mainly, when the bars in the corner boundary elements fractured it caused a noticeable strength diminishment. Moreover, for all the three specimens, it was noticed that most of the vertical reinforcement both in the web and flange regions outside the boundary elements ruptured at the connections between the wall and footing before any strength loss. During the following lateral displacement cycles in the strong axis (X-direction), rupture of vertical reinforcement resulted in sliding at the wall-foundation interface. This sliding factored in a remarkable portion of the total wall displacement, leading to out-of-plane bending of flanges, dowel action of boundary element reinforcement, and separation of corner boundary elements from the web.

The development of the damage was the same across all specimens. The flexural strength of the three walls was almost identical. After reaching the point of maximum strength in the strong axis (X-direction) loading, the response was controlled by weak-axis loading, which negatively affected the drift capacity and the stiffness during unloading-reloading cycles.

(a) West flange (b) Web (c) East Flange

Figure 2.11 Typical failure of the three walls (Lowes et al., 2014)

2.1.4. (Constantin & Beyer, 2016) : U-shaped Wall Test

At EPFL in Lausanne, Switzerland, a new test campaign was carried out on two U-shaped walls (TUC and TUD) which were tested to extend the research carried out by Beyer et al. (2008). This campaign focused on identifying the failure mechanisms of U-shaped shear walls subjected to diagonal loading and identifying the possible crucial design features in relation to these failure mechanisms.

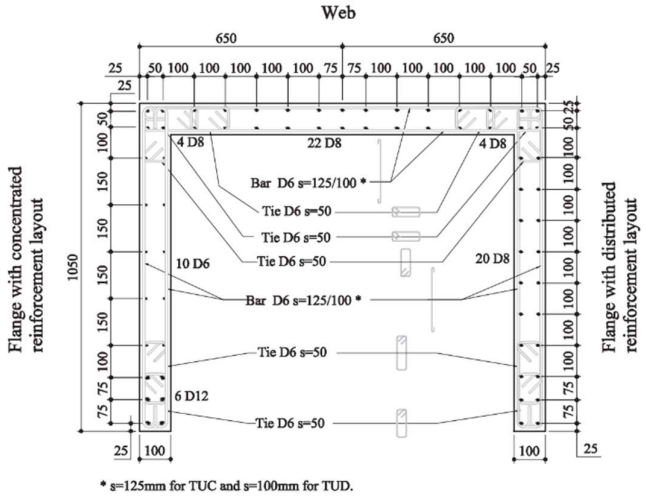

Figure 2.12 Cross section of the test specimen TUC and TUD scale 1:2. Dimensions in mm. (Constantin & Beyer, 2016)

The two test specimens were almost identical but only varied in the axial load ratio from $0.06.f'_c.A_g$ for TUC and $0.15.f'_c.A_g$ for TUD. The specimens were not specifically designed to comply with any specific design code. Moreover, to examine the effect of vertical reinforcement distribution one flange is detailed containing highly reinforced boundary element and the other flange was detailed with uniformly distributed reinforcement, while the web is also detailed with uniformly distributed reinforcement. Since the main objective was studying the behavior of the U-Shaped wall under diagonal loading, the primary loading cycles were applied along the geometric diagonals over increasing ductility levels.

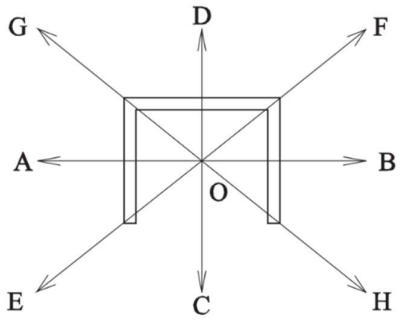

Figure 2.13 Loading path for TUC and TUD

Based on the experimental observations, The researchers concluded that the plane section assumption is not applicable for U-shaped walls subjected to diagonal loading as it misses to take into account the full compression zone between the web and flange intersection. In addition to that, they also observed that the diagonal loading scenario when one of the flanges ends is under compression gives the largest compression depth. This was clear from the strain distribution profiles at the base of the wall that were drawn from the readings of LVDT during the experiment at the base of the wall. As a recommendation, the length of the boundary element should be considered based on this loading case.

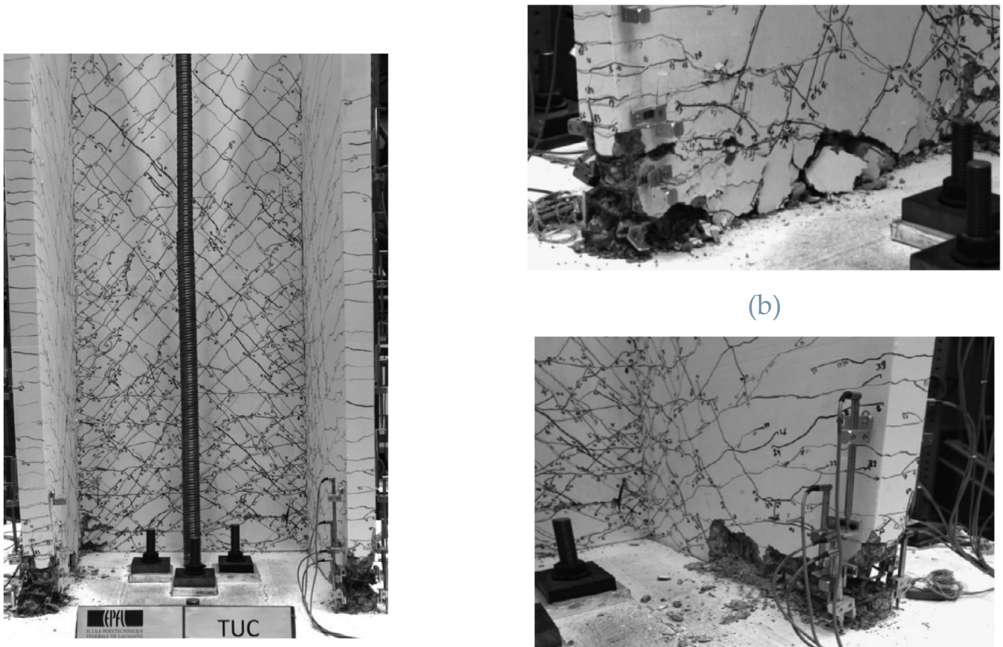

(a)

(b)

(c)

Figure 2.14 Failure of TUC (Constantin & Beyer, 2016)

a)Overall Cracking pattern, b)West flange (Concentrated reinforcement) , and c)East Flange (distributed reinforcement)

2.1.5. (Thomsen & Wallace, 2004): T-shaped Wall Test

At University of California, Los Angeles (UCLA), a test program of two quarterly scaled T-shaped walls was carried out. The walls were tested in order to better understand the application of the displacement-based design provisions, which developed at the beginning of the 1990's (Wallace & Moehle, 1992). This test focused on fixing the deficiencies of strength focused design provisions of the structural walls that are subjected to seismic loading.

The two test units were designed to reach an equal target drift of 1.5%. For TW1, it was detailed to have four boundary elements that are similar in the geometry and reinforcement detailing. For TW2, it was detailed with an increase of the transversal reinforcement with a deeper boundary element on the web toe in order to account for the deep compression depth in the case of loading the flange in tension.

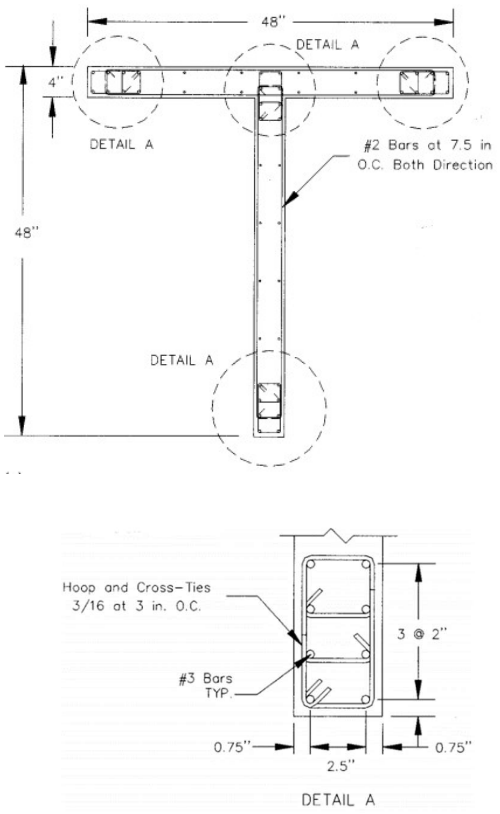

(a) TW1

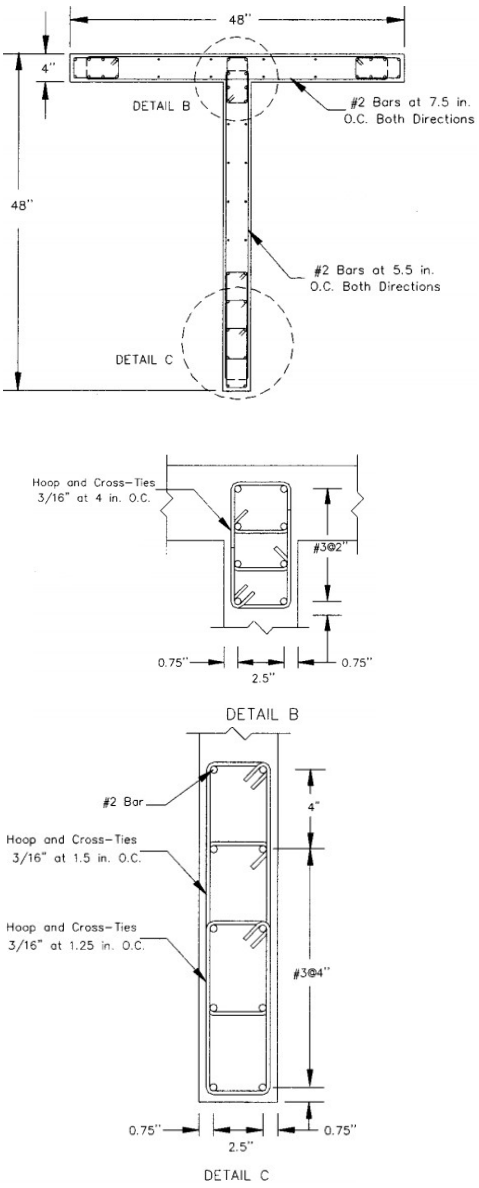

(b) TW2

Figure 2.15 Cross section of the test specimens by (Thomsen & Wallace, 2004) scale 1:4. Dimensions in inches.

The test units were assessed in an upright position, under constant axial load which is equivalent to $0.1.f'_c.A_g$ applied at the top of the wall. Reverse cyclic lateral displacements were imposed through hydraulic actuator which was fixed in a horizontal direction to a reaction wall at a level of 12ft from the base of the wall.

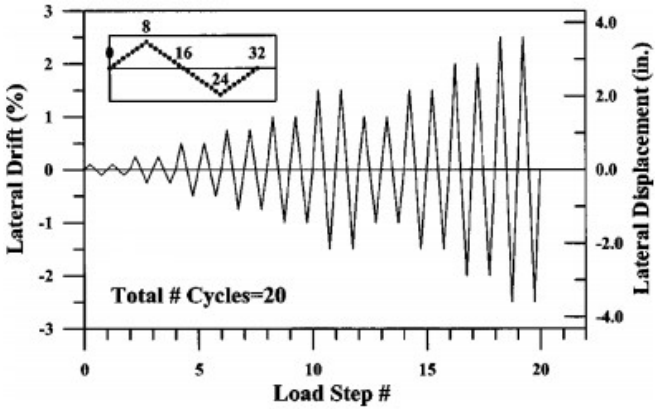

Figure 2.16 Loading History for TW1 and TW2

Based on the observation of the test results, TW2 which was detailed using the displacement-based design had a greater lateral capacity drift of average 2% which was only required to reach 1.5% by design. TW2 showed an excellent behavior during testing due to the tight spacing of the transverse reinforcement in the highly strain zones, but the lateral load capacity was limited by out of plane buckling. On the other hand is the brittle failure of TW1 due to poor detailing; it failed to reach the nominal moment of resistance.

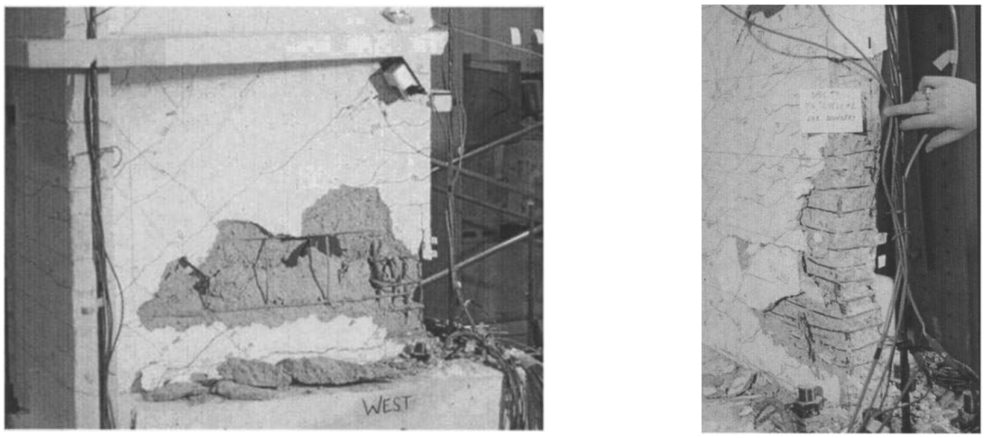

(a) (b)

Figure 2.17 Failure of TW1 and TW2 (Thomsen & Wallace, 2004)

a)Brittle failure of TW1, and b)Out-of-plane buckling of TW2

2.1.6. (Brueggen & French, 2009): T-shaped Wall Test

Two T-shaped walls (NTW1 and NTW2) that represented six-story-prototype structure were tested at the University of Minnesota under complicated multi-directional loading. Although, NTW1 was a four-story-test specimen while NTW2 was a two-story-test specimen. Each of the two specimens were subjected to an axial load at the top of the wall equivalent to $0.03.f'_c.A_g$ and moment to correspond to the six-story building.

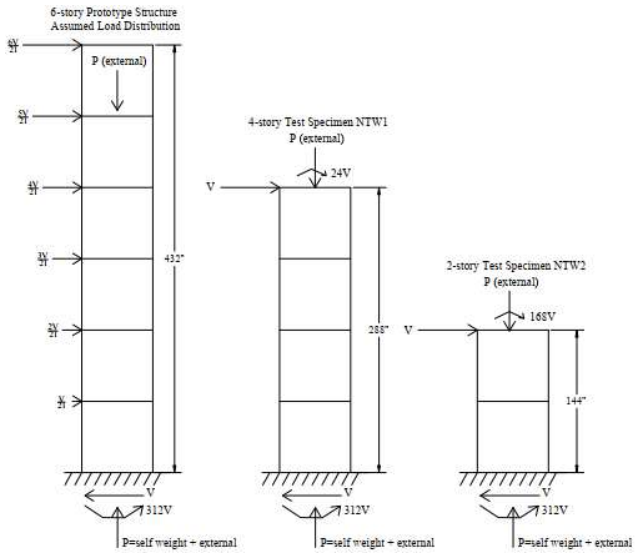

Figure 2.18 Loading of prototype structure and specimens

The two specimens were designed and checked to fulfill all the minimum and maximum requirements of ACI 318-02 in the spacing and dimensions except for the concrete cover and the confinement hoop spacing which were considered by the scaled design. It was also checked that the shear reinforcement was considered adequate to ensure the flexural failure of the walls.

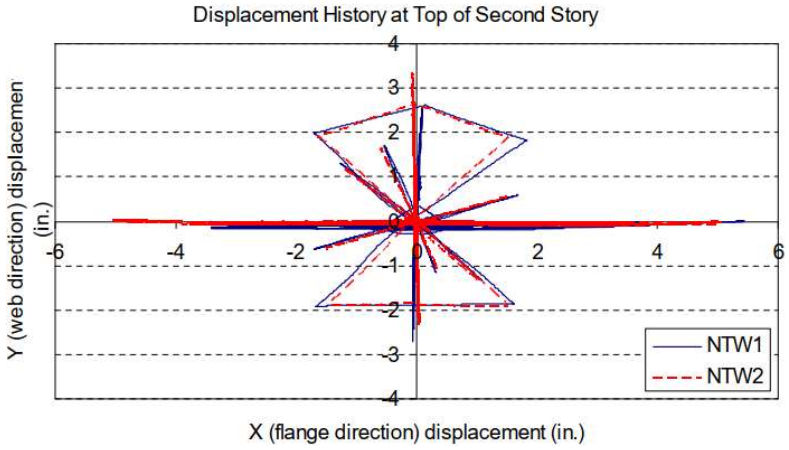

Figure 2.19 Loading path for NTW1 and NTW2

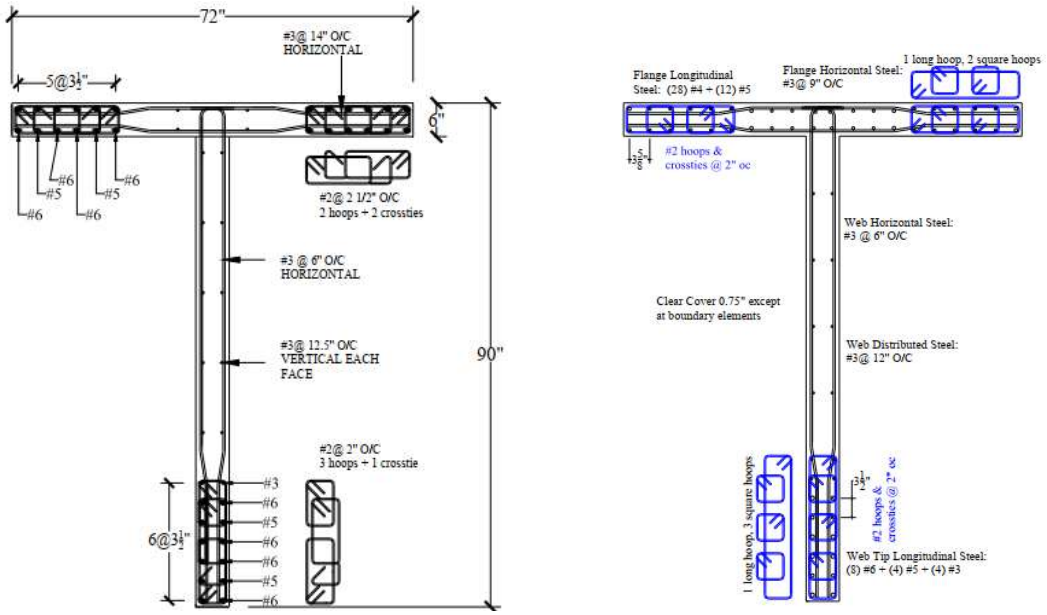

(a) Specimen NTW1 (b) Specimen NTW2

Figure 2.20 Specimen NTW1 and NTW2 geometry and reinforcing. Dimensions in inches. (Brueggen & French, 2009)

By concluding the test results, the researchers assured that i) the displacement-based design which is defined in the ACI 318-02 was adequate for the design of T-shaped walls under the bi-directional loading because the test units maintained strength out to the design drift demand. On the other hand, the ACI 318 displacement-design based procedure was considered inadequate to satisfy the requirements of the tension-controlled section because of the large compression depth in the case of the flange is under tension. So, the displacement-design based procedure failed to be adequate for the design. ii) The shear deformation played a vital role in the behavior of the wall in terms of stiffness and strength. By imposing high drift demands, the longitudinal reinforcement allocated in the effective flange width reaches the yield strain. But on applying low drift demands, the strain values at the flange ends could only reach half the strain value of the strain of the center of the flange. By which the strain distribution is affected mainly by the distribution of the longitudinal reinforcement over the cross section. iii)there must be a future additional test for non-planar walls with different geometry proportions, different values of axial load applied and different shear spans (M/V) ratios to better understand the behavior of the wall under any loading protocol and the shear lag effect.

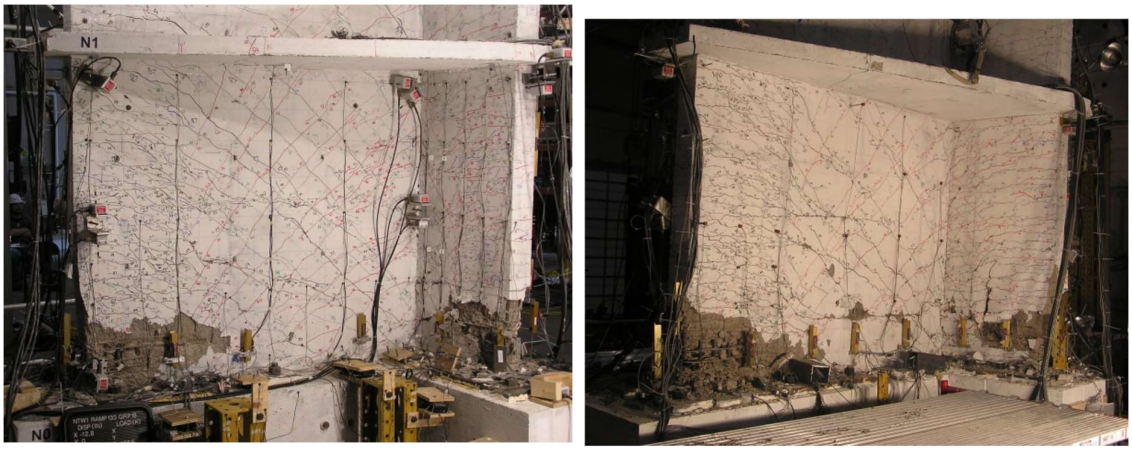

(a) NTW1 (b) NTW2

Figure 2.21 Failure of NTW1 and NTW2 (Brueggen & French, 2009)

2.1.7. (Inada et al., 2008): L-shaped Wall Test

Three reinforced concrete L-shaped walls (L00A, L45A and L45b) were tested at Kyoto University, statically loaded to study the behavior of the walls under different loading directions. The unit tests were 1:4.5 scale where they present the bottom of three stories of the wall system of a 40-story prototype structure. The height of the three units were considered 2.48m from the top face of the foundation. Two of the walls were equilateral L-shaped walls (L45A and L00A), while the third L-shaped wall was inequilateral (L45B). The three test units were of the same thickness, which is equal to 200mm, in addition to the steel reinforcement ratios which were equivalent for the three walls either in the confined or unconfined zones.

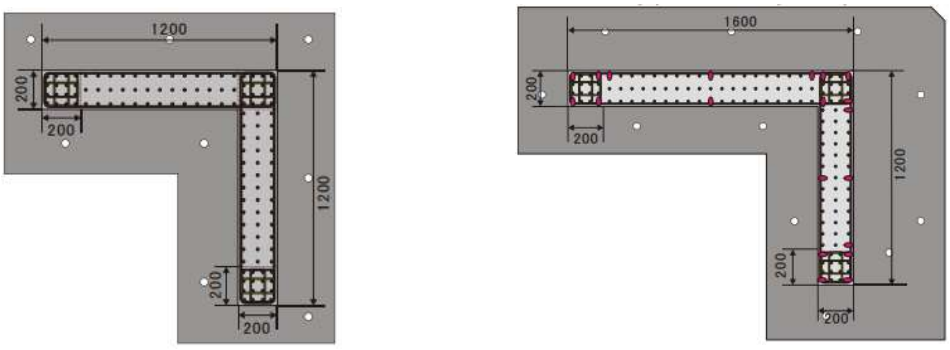

(a) L00A, L45A (b) L45B

Figure 2.22Cross Section of test specimen scale 1:4.5. Dimensions in mm. (Inada et al., 2008)

They were tested under static unidirectional cyclic loading. But for wall L00A was loaded parallel to on flange while for L45A and L45B, they were both loaded at an angle 45 degrees. Not only the static cyclic unidirectional loading, but also, they were subjected to an axial load ratio that varies along the test. For L00A, it varied from 0 (when the flange tips were in compression) to $0.31.f'_c.A_g$, while for L45A and L45B varied from 0 to $0.26.f'_c.A_g$.

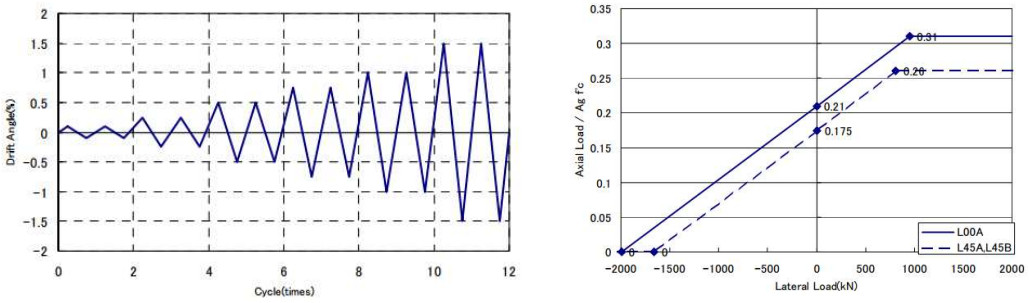

(a) Cyclic Lateral Loading (b) Axial Loading

Figure 2.23 Loading Path (Inada et al., 2008)

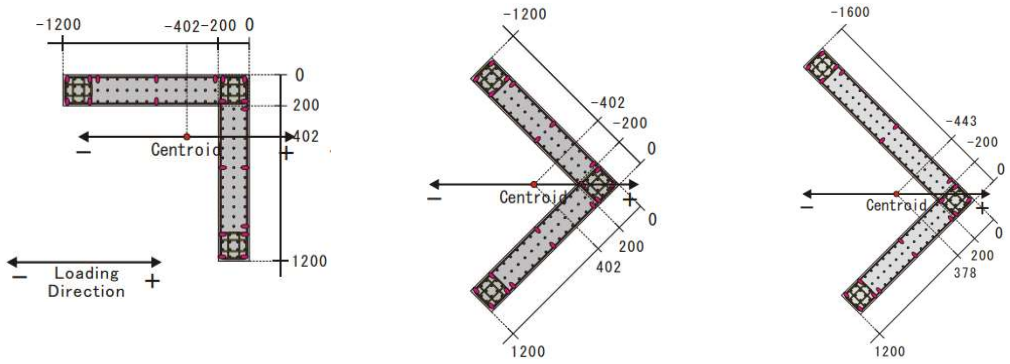

(a)L00A (b)L45A c)L45B

Figure 2.24 Loading Direction

The three test units failed in a compression-controlled flexural behavior which was shown in the crushing of the concrete and the buckling of the reinforcement bars in the walls' corners, specifically in the unconfined zones the compression damage was extreme. The behavior of the walls was noted down during the test and the researchers concluded that for the test units that were loaded at angle of 45 degrees, when loading the end of the flange in compression and the corner in tension, the strain distribution at the base of the wall was considered linear. While in loading the end of the flange in tension and the corner in compression, there was a non-linear strain distribution that was clear just at the yielding of the steel and the crushing of the concrete.

(a)L00A

(b)L45A

(c)L45B

Figure 2.25 Failure of the Walls (Inada et al., 2008)

2.1.8. (Li & Li, 2012) :L-shaped Wall Test

In the Chinese construction market, there is a large-scale usage of short-limbed L-shaped walls "SLW" (Length to thickness ratio from 5 to 8 and thickness more than 200mm, as they grant more lateral stiffness than that of the frame system, while also gives more flexibility in the usage of the floor area, their structural seismic performance of such walls is however still unclear. For this reason, testing of 4 SLWs was done by (Li & Li, 2012) at the Xi'an University to get more knowledge about the non-linear behavior and ductility capacity of these type of walls.

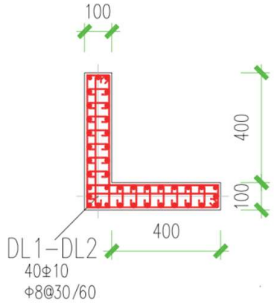

(a)

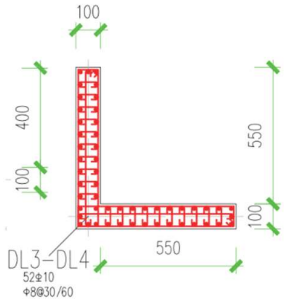

(b)

Figure 2.26 Cross section of the test specimens by (Li & Li, 2012) scale 1:2. Dimensions in mm.

The testing campaign targeted to study the effect of axial load ratio and the length to thickness on the seismic performance, the four test specimens were scaled 1:2 with the same flange length. All the test specimens are longitudinally reinforced uniformly and the whole section is confined with transverse reinforcement. Wall DL1 and DL2 were built to have a length to thickness ratio equal to 5 while DL3 and DL4 were built to have a ratio equal to 6.5, Cross sections are shown in Figure 2.26. All the test specimens were subjected to quasi-static cyclic latera loading in one direction in the direction of one of the flanges. In addition to that, each wall was subjected to constant axial load throughout the test. The values of the axial load ratios are shown in Table2.1.

Specimen No.	Axial Load Ratio
DL1	0.3
DL2	0.4
DL3	0.2
DL4	0.1

Table 2.1 Axial load ratio for L-shaped walls

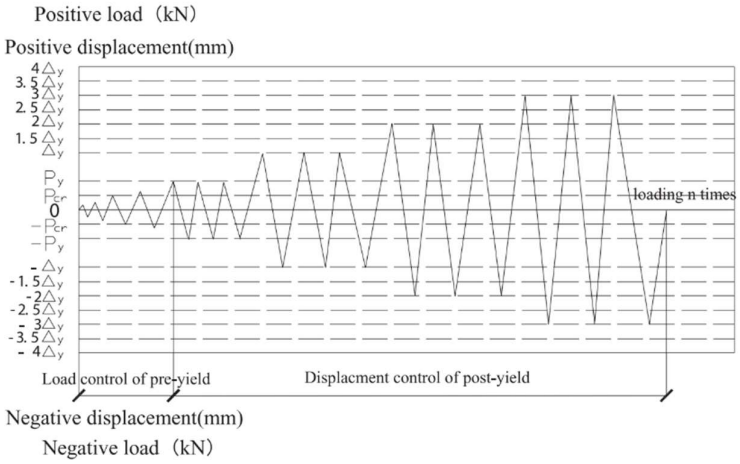

Figure 2.27 Loading History for DL1-DL4

from the test results (Li & Li, 2012) noted that the walls failed in compression at the extreme ends of the flanges by crushing of concrete and buckling of longitudinal reinforcement. Moreover, asymmetric load displacement response which was anticipated to the asymmetry in the cross-section and the asymmetric behavior was more shown by the difference of the axial load. Ductility capacity was enhanced by the cutback in axial load and length to thickness ratio, while the energy dissipated increased a bit with the increasing length to thickness ratio. Finally, the results showed a better behavior of the traditional shear walls.

(a) (b)

Figure 2.28 Failure of DL2 (Li & Li, 2012)

2.1.9. (Oesterle et al., 1976, 1979) :H-shaped Wall Test

The Test campaign done by researchers at the Portland cement Association comprised two H-Shaped shear walls (F1 and F2) to increase the understanding of this type of walls. F1 was reinforced with 3.89% longitudinal reinforcement and was not loaded axially, while F2 had a higher longitudinal reinforcement ratio of 4.35% and loaded axially with a value of $0.07.f'_c.A_g$. F1 was detailed in a way that the whole flange was considered to be a confined zone as shown in Figure 2.29a, F2 was detailed to have a confined zone the web-flange interconnection only as showing in Figure 2.29b. ACI-1971 was used as a design code for the designing and detailing of the two walls in shear and flexure.

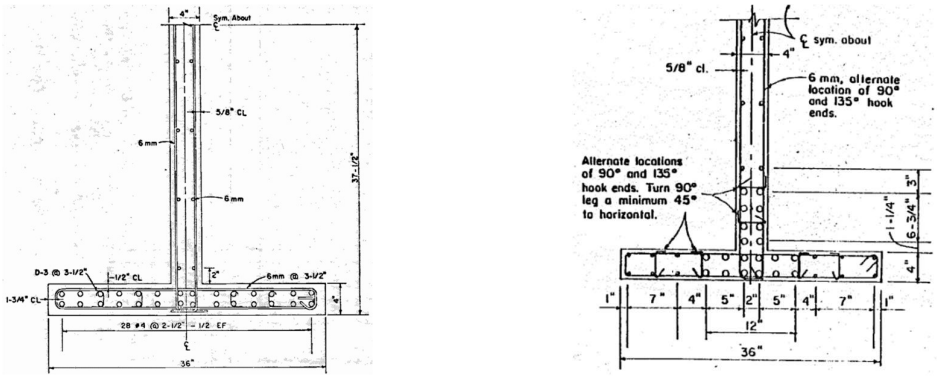

(a)F1 (b)F2

Figure 2.29 Cross sections of H-shaped Shear walls done by (Oesterle et al., 1976, 1979). Dimensions in inches.

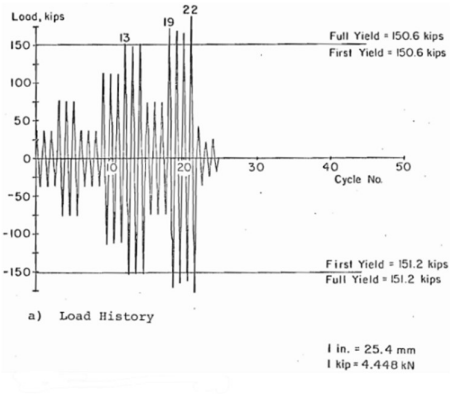

(a) F1

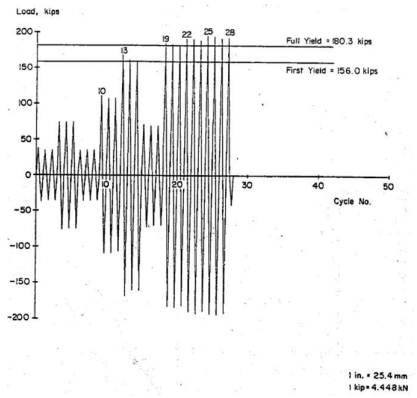

(b) F2

Figure 2.30 Loading history for the tests done by (Oesterle et al., 1976, 1979)

The two specimens failed due to crushing of concrete in the unconfined zone in the web near the web-flange interconnection and this was related by the researchers to the high shear forces at the connection between the web and flange resulting for the small compression zone developed at the intersection. The reinforcement of the confined zones/boundary elements postponed the crushing of the concrete by providing more stability to the bars preventing the delaying the buckling of the longitudinal bars.

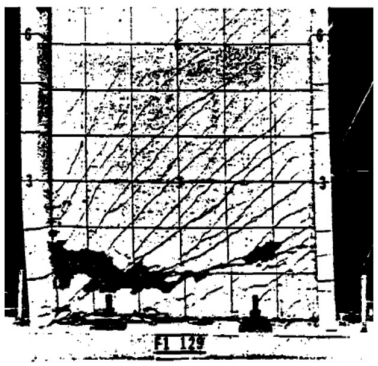

(a)

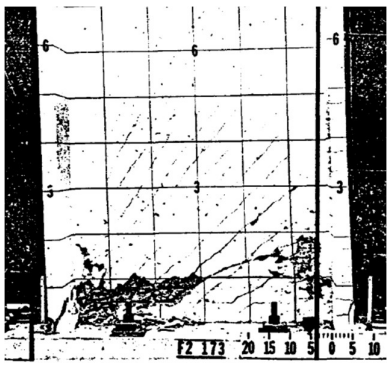

(b)

Figure 2.31 Failure of H-shaped Shear Walls done by (Oesterle et al., 1976, 1979)

Web Crushing Failure of a)F1 and, b)F2

2.2. Summary of Test Campaigns

Test Campaign	Test Unit	Type	Lateral Loading Direction		Axial Load Ratio	Vertical Reinforcement	Horizontal Reinforcement
			Unidirectional	Bidirectional			
(Ile & Reynouard, 2005)	IleX	U	✓		0.1	0.56%	0.39%
	IleY	U	✓				
	IleXY	U		✓			
(Beyer et al., 2008b) (Constantin & Beyer, 2016)	TUA	U		✓	0.02	0.71%	0.3%
	TUB	U		✓	0.04	1.01%	0.45%
	TUC	U		✓	0.06	1.09%	0.45%
	TUD	U		✓	0.15	1.09%	0.57%
(Lowes et al., 2014)	CW1	C	✓		0.05	0.79%	0.65%
	CW2	C		✓			
	CW3	C		✓			
(Thomsen & Wallace, 2004)	TW1	T	✓		0.1	1.17%	0.33%
	TW2	T	✓			1.2%	0.45%
(Brueggen & French, 2009)	NTW1	T		✓	0.03	2.51%	0.26%
	NTW2	T		✓		2.16%	0.41%
(Oesterle et al., 1976, 1979)	F1	H	✓		-	1.55%	0.71%
	F2	H	✓		0.07	1.26%	0.63%
(Inada et al., 2008)	L00A	L	✓		varies: 0-0.31	3.80%	0.89%
	L45A	L	✓		varies: 0-0.26	3.80%	
	L45B	L	✓		varies: 0-0.26	4.34%	
(Li & Li, 2012)	DL1	L	✓		0.3	3.90%	0.34%
	DL2	L	✓		0.4		0.17%
	DL3	L	✓		0.2	3.70%	0.34%
	DL4	L	✓		0.1		0.17%

Table 2.2 Summary of Test Campaigns

2.3. Modeling Approaches of non-planar composite Shear walls

2.3.1. Simplified Models

Simplified models for analyzing reinforced concrete (RC) walls generally depends on empirical data, mechanical principles, or an integration of both. The plastic hinge model is one of the most used simplified models. It relies on the concept that the force-displacement behavior of an RC wall forming a flexural mechanism can be obtained from the section's moment-curvature relationship experiencing the highest moment demand. Consequently, shear force is calculated by dividing the moment by the shear span, calculating the displacements using the curvatures needs some calculations(Constantin & Raluca-Tereza, 2016).

The calculation of flexural displacement includes the sum of both elastic and plastic displacements. The elastic displacement is approximated using the wall's yield displacement (Δ_y). Along the shear span, linear approximation of elastic curvatures (curvatures less than the yield curvature (ϕ_y) are considered. Plastic curvatures are condensed within a specific zone named as the equivalent plastic hinge length; these are assumed to be constant. Integrating these assumed curvature profiles over the wall's height gives us flexural displacements. In the plastic hinge model, displacements resulting from strain penetration into the foundation are taken into account within flexural displacements. This is attained by including a strain penetration term in the equation for plastic hinge length, by which the equation takes into account the plastic flexural deformation. Shear displacement displacements (Δ_s) can be combined with the flexural displacements (Δ_f) through semi-empirical models correlating shear and flexural deformations which were newly proposed by (Beyer et al., 2011).

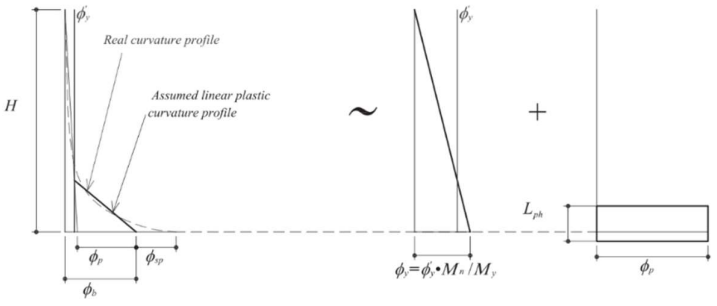

Figure 2.32 Linear approximations of the curvature profile and the plastic hinge model (Constantin & Raluca-Tereza, 2016)

$$\Delta = \Delta_y + \Delta_p \quad \text{Eq. 2.1}$$

$$\Delta_y = \phi_y \frac{H^2}{3} \quad \text{Eq. 2.2}$$

$$\Delta_{p,f} = \phi_y . L_{ph} . H \quad \text{Eq. 2.3}$$

$$\Delta = \Delta_y + \Delta_{p,f}(1 + \frac{\Delta_s}{\Delta_f}) \quad \text{Eq. 2.4}$$

2.3.2. Macro Models

2.3.2.1. Beam-column element models

In models using beam-column elements, the wall section is generally modelled by a single type of element. Primary concerns while defining these types of models are the element formulation of the beam column element and the discretization decisions, such as the number of elements along the wall height. The number of integration points per element and the element discretization are mainly affected by the choice of the element formulation.

Two categories of beam elements are differentiated based on their formulation: displacement-based and force-based elements. For displacement-based elements, the displacement field is enforced, and forces are evaluated using energy balance considerations. On the contrary, force-based elements enforce the force field, and element displacements are evaluated through work equivalence balance (Calabrese et al., 2010). Displacement-based elements usually assume linear variation of curvature over the element height, while force-based elements assume linear variation of moment over the wall height. In order to have a realistic modeling of the wall it is recommended to have multiple displacement-based elements along the height; however, a single force-based element is sufficient for the same effect. Nevertheless, displacement-based elements are more widely spread in the real-world application(Calabrese et al., 2010) (Arabzadeh et al., 2017).

A displacement-based formulation uses an interpolation of displacements or curvatures over a fiber element, which may not accurately be present to show the high nonlinear behavior. displacement-based solutions can be enhanced by elevating the mesh density, leading to an increase in the computational cost. The force-based formulation is generally opted since the interpolation functions it uses correspond to the accurate solution of the internal forces in the elements. Nevertheless, Force-based elements uses the plane section assumption which fails to accurately capture the shear and flexural interaction deformation(Arabzadeh et al., 2017).

To be able to model the wall behavior, the beam column elements have the feature of distributing the plasticity along the element length, axial flexural interaction is captured due to the usage of fiber sections which are assigned to them. Shear displacement is commonly either neglected or modeled with a linear elastic displacement, which in order decouple the shear and flexural behavior(Correia et al., 2015).

Material models assigned to the fiber sections are often uniaxial, so easy to represent. But special concrete behavior like confinement needs to be simplified in order to be modelled correctly. Planar reinforced concrete wall behavior can be reasonably accurately estimated using beam-column models, On the other hand, for non-planar walls, fiber sections cannot differentiate the shear forces between the different wall

elements (flanges and web). One of the main pros of using beam column elements is the low computational cost.

2.3.2.2. Wide-column models

In the wide-column analogy, non-planar walls can be separated into web and flange segments. These segments are represented by vertical beam elements centered along each of the web and flange segments. Afterwards, these beam elements are attached through horizontal links aligned with the weak axes of the sections, by which a common node is located at the intersection between the web and flange segments for the connection.

The Wide-Column Model (WCM) is considered as a simple and direct approach that is used for modeling non-planar walls. It provides a clear method for determining the distribution of shear forces among the wall components as the web, and each of the two flanges for the case of U-shaped walls. The setting up of the model is simple and easy, the low computational cost is low, so it is a viable choice for modelling of non-planar walls with irregular geometries (Arabzadeh et al., 2017).

Since the fiber elements are rigid in shear and torsion, they consider only flexure and compression. To solve this issue, the contribution of the horizontal steel rebars in the shear resistance of the core is considered by highly rigid springs that are placed in a certain way to simulate the shear deformation at these specific locations and can be applied in between the members of the WCM. More detailed research on WCM was done by (Beyer et al., 2008a) and (Arabzadeh et al., 2017).

2.3.3. Detailed Finite Element Models

Detailed Finite Element (FE) models are known to be the most advanced modeling approach but also the highest computationally demanding approach. Due to their complexity, these models are bound to represent planar walls.

On the other hand, Shell finite elements offer a much simpler and reduced computational effort, making them a better choice when simulating RC wall behavior. These elements show their benefits when the wall's out-of-plane behavior is crucial to be studied. These types of elements take into account axial, flexural, shear, torsional behavior, and the interaction between them. Material models that could be used in a detailed FE model could be a two or a three-dimensional constitutive law which increases the refinement of this type of model.

Despite the advantages provided with the FE approach, they have their cons. The main limitation is the huge computational time needed and the importance of post-processing to calculate the straining actions required to design. Another complexity is the ability to calculate the parameters needed to represent the material models.

3 Quasi-static Tests of U-shaped Walls

3.1. Introduction

This chapter discusses the testing done by (Beyer et al., 2008b) & (Constantin & Beyer, 2016) for test units TUA, TUB and TUC which was subjected to different loading scenario to study different hysteretic behavior of the U-shaped walls. Later, these experimental results will be compared to the numerical results coming from the OpenSees software.

3.2. Test Units and Test Setup

3.2.1. Geometry of the Test Units

The three test units were scaled to half their original dimensions as they were representing an elevator shaft. For TUA and TUB the main difference was the thickness of the walls which was 0.15 m for TUA and 0.1 m for TUB which reflects 0.3 and 0.2 in the full-scale walls. Wall thickness was chosen to be the main variable to be changed by keeping everything else constant. It was anticipated that it will affect the overall behavior of the wall such as shear load carrying capacity, length of the compression zone and strain demands. As for the reinforcement of TUA and TUB they nearly have the same vertical and horizontal reinforcement areas. For TUC, the thickness of the wall was 0.1 m which was similar to TUB. It was different in a unique way that the vertical reinforcement layout was decided to be different in both flanges. The left flange was detailed with vertical reinforcement that was concentrated in the boundary element, while the right flange had a uniformly distributed reinforcement layout. This change was done to study the effect of the vertical reinforcement layout on the behavior of the wall.

Regarding the three test units, unreinforced concrete studs were added to the base of wall to act as shear keys to increase the connection between the wall base and the foundation and increase the resistance against to shear sliding.

	TUA	TUB	TUC
Scale	1:2	1:2	1:2
Compactness ratio:			
l_{web}/t_w	8.7	13	13
l_{fl}/t_w	7	10.5	10.5
Vertical reinforcement ratio:	0.71%	1.01%	1.09%
Horizontal reinforcement ratio:			
web:	0.3	0.45	0.45
flange:	0.3	0.45	0.45

Table 3.1 Comparison of cross sections of TUA, TUB, and TUC

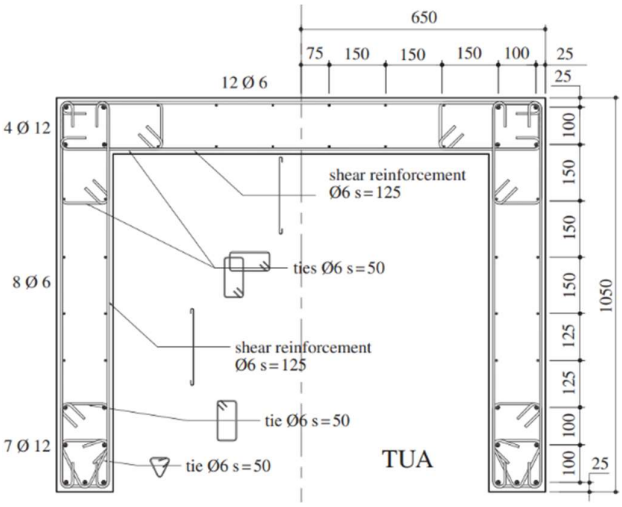

Figure 3.1 Cross section of the test specimen TUA scale 1:2. Dimensions in mm.(Beyer et al., 2008b)

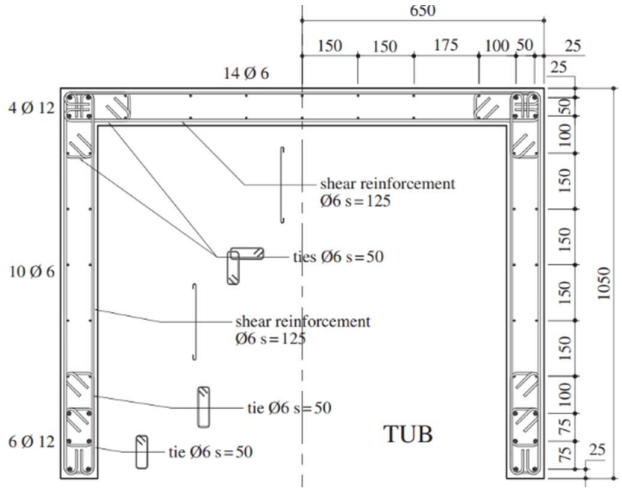

Figure 3.2 Cross section of the test specimen TUB scale 1:2. Dimensions in mm.(Beyer et al., 2008b)

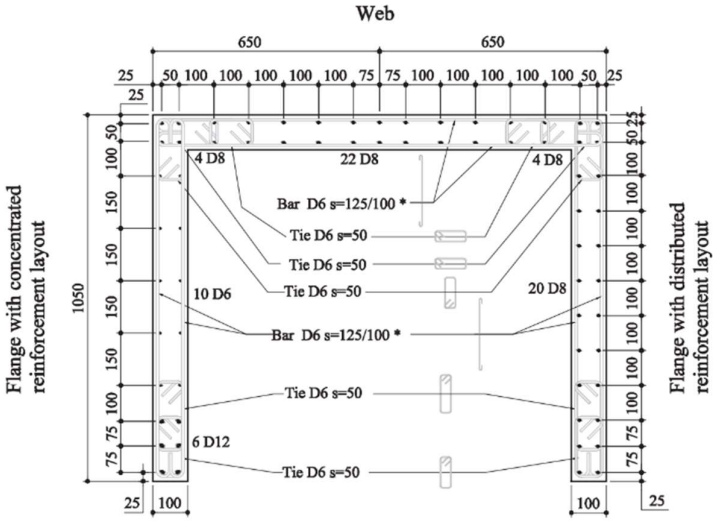

Figure 3.3 Cross section of the test specimen TUC scale 1:2.
Dimensions in mm.(Constantin & Beyer, 2016)

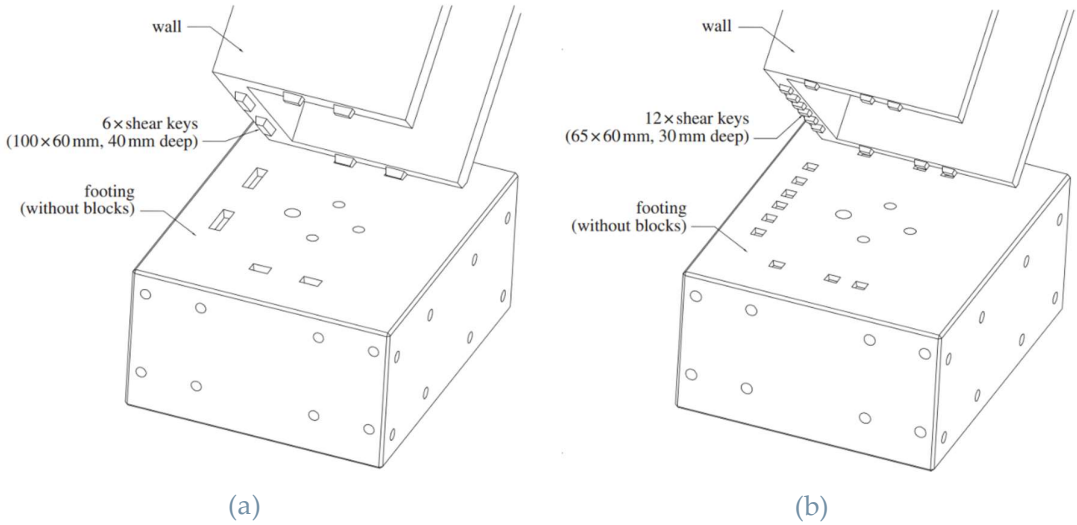

Figure 3.4 Shear keys distribution (Beyer et al., 2008b)

a)TUA, b)TUB & TUC

3.2.2. Material properties

3.2.2.1. Reinforcement steel

For TUA and TUB all the reinforcement steel bars D12 and D6 were in compliance with "Class C" grade according to (EC8, 2004) For TUC, D12 and D8 bars were "Class C" while D6 bars were "Class B", where D refers to the bar diameter. All the steel

properties were acquired by monotonic tensile testing at the day of testing and are mentioned in Table 3.2.

	f_y [MPa]	f_u [MPa]	f_u/f_y	ε_{su} [%]
TUA: D12mm bars	488	595	1.22	12.6
TUB: D12mm bars	471	572	1.21	12.7
TUA & TUB: D6mm bars	518	680	1.31	8.4
TUC: D12mm bars	529	633	1.19	9.6
TUC: D8mm bars	563	663	1.18	7.9
TUC: D6mm bars	492	623	1.26	6.8

Table 3.2 Reinforcing steel properties for TUA, TUB ,and TUC

3.2.2.2. Reinforced Concrete

For the three test units' compressive strength was determined based on a concrete compressive test at 28 days and at the day of testing and the properties mentioned in Table 3.3.

	28 Days	Day of testing		Double-punch test
	f'_c [MPa]	f'_c [MPa]	E_c [MPa]	f'_t [MPa]
TUA	77.3	77.9	37	5.95
TUB	48.1	54.7	33.5	4.25
TUC	38.1	42	31.6	3.2

Table 3.3 Reinforced concrete properties for TUA, TUB and TUC

3.2.3. Description of test setup

This section gives a detailed view of the setting up of the test units and how the instruments are being adapted to be able to reach the objective of the experimental test.

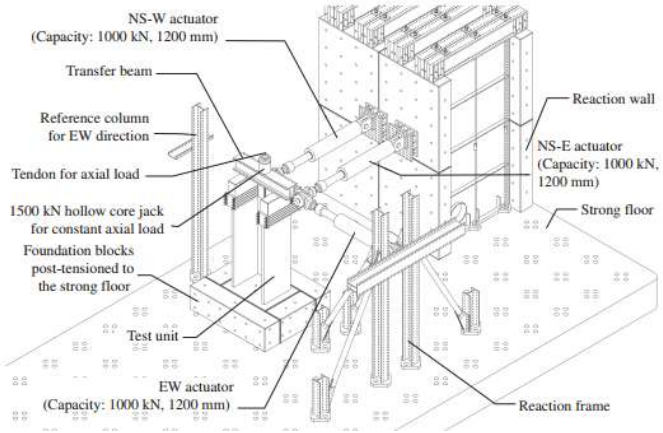

Figure 3.5 Isometric View of the Test Setup. (Beyer et al., 2008b)

An overall isometric view of the test setup is shown in Figure 3.5 and Figure 3.6 shows the test setting up of the test.

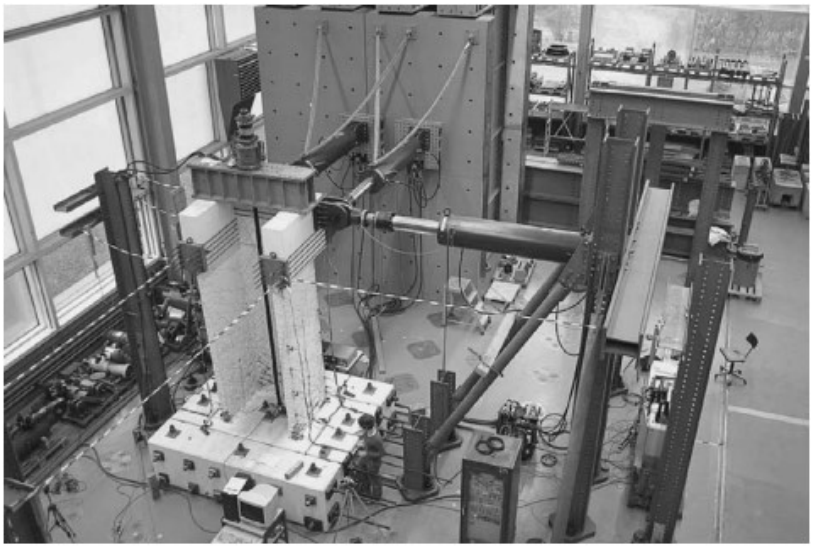

Figure 3.6 Test Setup (Beyer et al., 2008b)

The test was performed in displacement control and rotation of the top of the wall. So, each test unit was loaded by three actuators, in order to control the two translational degrees of freedom and twisting of the test unit from its head. There were two actuators in the NS direction which loaded the two flanges. While the actuator in the EW direction loaded the web of the wall. The orientation of the test units with respect to the cardinal points, a detailed identification of each of the web and flanges regions and the line of action of each actuator are shown in Figure 3.7.

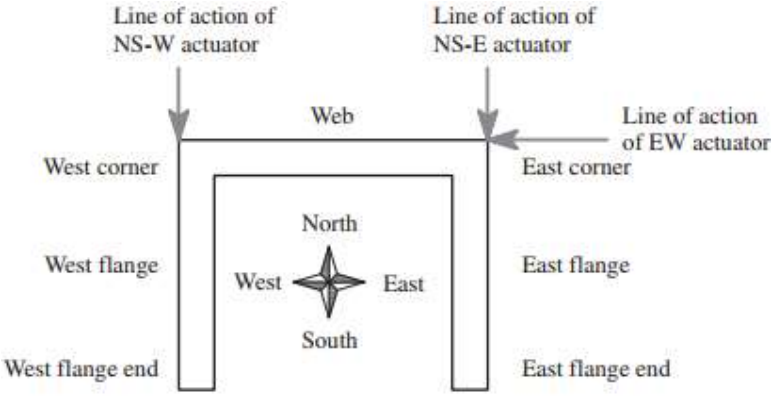

Figure 3.7 Location of the Actuators(Beyer et al., 2008b)

The location of the actuators was chosen based on various aspects. Firstly, the shear span was a factor behind the choice; as when dealing with the smallest shear span, we get the highest shear force demand for the same moment capacity. The latter condition allowed the testing of the walls under the highest estimated shear force during inelastic flexural deformations. Secondly, it was considered as a practical aspect by

trying to have similar heights of the actuators in the two principal directions to be able to manage the dimensions of the load stub to a practical size. The shear spans which are considered the same as the location of the actuators are listed in Table 3.4.

	TUA	TUB	TUC
Shear span h_{NS} [M/V]	2.95m	2.95m	2.95m
Shear span h_{EW} [M/V]	3.35m	3.35m	3.35m
Shear span ratio [h_{NS} /l_w]	2.81	2.81	2.81
Shear span ratio [h_{EW} /l_w]	2.58	2.58	2.58

Table 3.4 Location of the actuators for TUA,TUB and TUC

The axial load was placed on the top of the transfer beam at the top of the unit test. It was maintained constant throughout the test by the tendon which was pretensioned by hollow core jack. The hollow core jack was interconnected to a load follower which is responsible to have an applied constant load through the test.

3.2.4. Loading History

The two test units TUA and TUB were subjected to displacement control loading in all the five different directions to be able to study the behavior in each direction:

- E-W direction (Parallel to the web)
- N-S direction (Parallel to the flanges)
- Diagonal direction where one flange end in compression
- Diagonal direction where one corner in compression

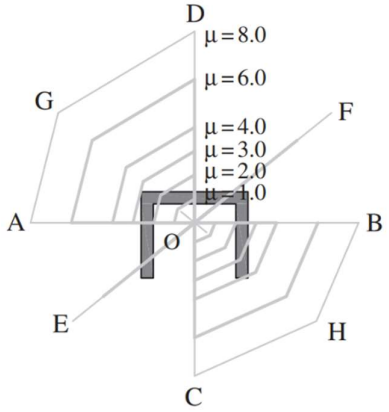

Figure 3.8 Loading path for TUA and TUB (Beyer et al., 2008b)

The E-W loading was controlled at a height of 3.35 m while the N-S loading was controlled at a height of 2.95 m, the loading pattern that was applied consists of a "sweep" and a diagonal at each ductility level. The pattern was created by (Hines et al., 2006) this loading pattern was applied to the wall after a complete cycle in E-W direction and a complete cycle in the N-S direction.

The loading history was composed of 8 ductility levels where the first 4 levels were in the elastic range and reflected a max of 25, 50, 75, and 100% of the forces leading to the yielding, respectively.

The details of the loading pattern for TUA and TUB are:

- EW cycle: (O → A → B → O)
- NS cycle: (O→ C → D → O)
- Diagonal cycle: full cycle in diagonal direction (O → E→ F→ O)
- ''Sweep'' (O → A → G → D → C → H → B → O)

In addition to the lateral loading the walls were subjected to a constant axial load of 780 KN which was similar to TUA and TUB during the whole testing, which represents 0.02 and 0.04 axial load ratio for TUA and TUB, respectively.

As for the test units TUC, it was primary laterally loaded in the two diagonal directions with an increasing ductility levels. It was subjected to a constant axial load of 820 KN which reflects an axial load ratio of 0.06.

The details of the loading pattern for TUC are:

- 0.1% drift: O → C → D → O → A → B → O.
- 0.2%drift:O → C → D → O → A → B → O → E → F → O → H → G → O.
- 0.3%, 0.4%, 0.6% drifts: O → E → F → O → H → G → O → C → D → O → A → B → O.
- 0.8% drift: O → C → D → C → D → O → A → B → A → B → O.
- 1.0%, 2.0% drifts: O → E → F → E → F → O → H → G → H → G → O.
- 1.5% drifts: O → H → G → H → G → O → E → F → E → F → O.
- 2.5% drift: O → H → G → O → E → F → O.
- 3.0% drift: O → E → O → H → O (loss of vertical load bearing capacity led to test stoppage).

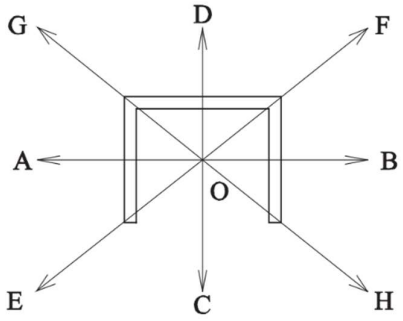

Figure 3.9 Loading Path for TUC

	TUA	TUB	TUC
Axial load [KN]	780	780	820
Axial load ratio	0.02	0.04	0.06

Table 3.5 Axial load for TUA, TUB, and TUC

3.3. Tests Results

3.3.1. Failure Mechanisms

3.3.1.1. TUA

The failure of TUA was mainly due to the fracture of the longitudinal reinforcement. Concrete spalling of the concrete cover was first noticed through the sweep part of the test at $\mu_\Delta = 3$. Although it was very limited at this point, it became more observable through the diagonal cycle of the $\mu_\Delta = 4$, during the diagonal loading at $\mu_\Delta = 6$ it was noticed buckling of the first longitudinal bar (D12) in the boundary element of the west flange (Position E). Fracture of two (D6) bars in the west flange during the E-W loading cycle at $\mu_\Delta = 8$ (Position B) these bars had buckled due to spalling of their concrete cover. The first buckled bar (D12) raptured during N-S loading cycle at $\mu_\Delta = 8$ (Position C to D). The diagonal cycle at $\mu_\Delta = 8$ was the last cycle that failure of the test unit since additional D12 bar and all the D6 bars left in the west flange were fractured (Position E to F).

(a) (b)

Figure 3.10 Failure of TUA (Beyer et al., 2008b)

a)Rupture of D12 longitudinal bars in the west flange, and b)crushing of the unconfined zones in the flange and the web

Compression concrete failure was not noticed in the behavior of TUA, only concrete spalling occurred. Concrete in the boundary elements remained intact while unconfined concrete zones of the flange and the web broke down. A regular crack pattern was formed in the web comparable to that of a planar wall subjected to cyclic loading, while a complex crack pattern developed in the flanges at different angles resulting from the complex bi-directional loading.

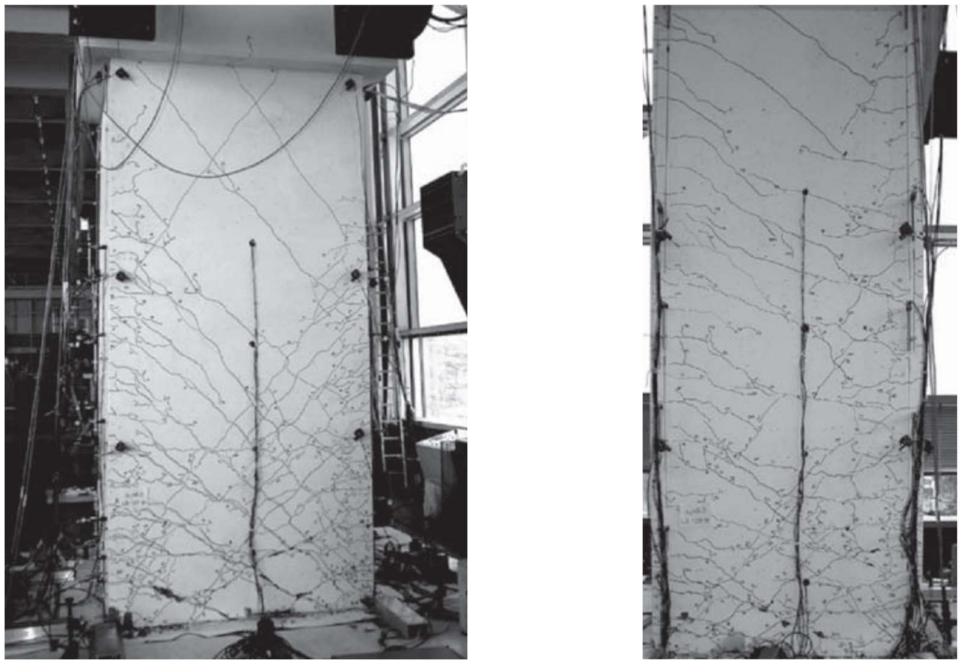

(a) Web (b) Flange

Figure 3.11 Crack Pattern of TUA (Beyer et al., 2008b)

3.3.1.2. TUB

Loss of the load carrying capacity was mainly due to the Crushing of the concrete compression diagonals of the unconfined zones in the web.

Concrete spalling of the concrete cover was first noticed at $\mu_\Delta = 2$, despite this longitudinal reinforcement was not exposed until $\mu_\Delta = 4$ during the N-S cycle. Concrete spalling originated at the boundary elements stretching to the unconfined zones owing to the bi-directional loading history applied, this led to a decrease in the wall width in the unconfined zone of the web causing the crushing failure of the web.

The boundary element played a vital role in making the failure of the of the wall not so tragic, as a part of the lateral load was well transferred to the boundary elements allowing for a frame mechanism. In this mechanism, the confined zones acted as short columns and the failing compression diagonal acted a beam.

(a) (b)

Figure 3.12 Failure of TUB (Beyer et al., 2008b)

a)Crushing of the unconfined zones in the web, and b)frame mechanism shown by the dotted lines

Unlike TUA, no steel reinforcement bars fractured during the test. However, buckling of two D12 bars in the west flange boundary element were noticed at $\mu_\Delta = 6$ during the diagonal cycle (Position E). Similar crack pattern was observed in TUB in comparison to TUA, by which the spacing of the cracks was less than that of TUA and some upper part of the wall was cracked.

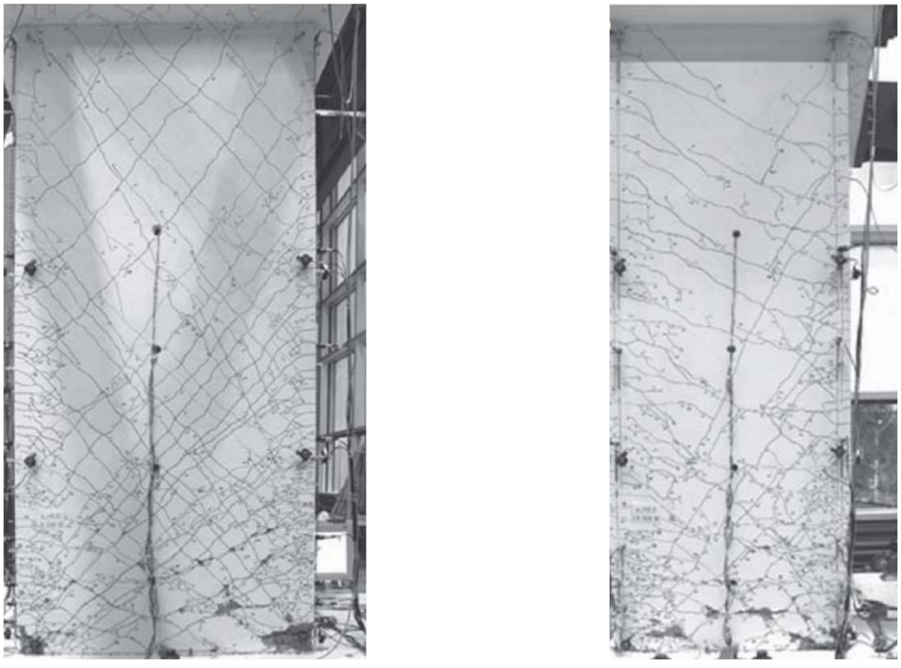

(a) Web (b) Flange

Figure 3.13 Crack Pattern of TUB (Beyer et al., 2008b)

3.3.1.3. TUC

TUC was not symmetric in the reinforcement details in the two flanges, where the east flange was constructed with distributed reinforcement, while the west flange was constructed with Concentrated reinforcement in the boundary elements. So, the behavior of the two flanges was not similar through the test. Therefore, discussion of the failure process, cracking pattern and influence of the reinforcement detail will be discussed for each flange separately.

(A) Failure of the West Flange (Concentrated reinforcement)

During loading in the E to F diagonal direction, the west flange failed as result of out of plane buckling leading to compression failure (Position E). Wall stiffness dropped through loading from O to E in comparison with previous cycles, a 35% drop of load carrying capacity was noticed comparable to the last cycle at the same position.

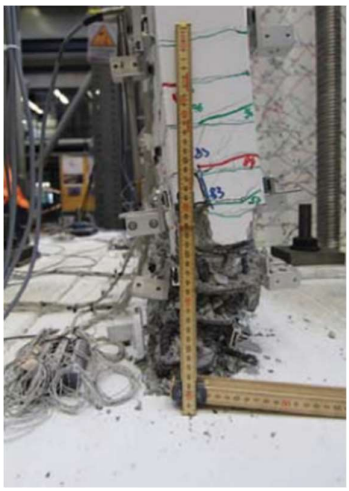

(a)

(b)

(c)

Figure 3.14 Failure of the West Flange TUC (Concentrated Reinforcement) (Constantin & Beyer, 2016)

a)Out of plane Buckling of the West Flange, Concrete Compression failure (Crushing) b) Outside view, and c) Inside View. At SRSS drift = 1% Position E

The out of plane buckling resulted from the largely imposed displacement history applied at position F, high tensile strains evolved in the boundary elements' reinforcing steel bars causing a spread of large cracks in this zone of approximately 4 mm width. During unloading from F and loading to position E the vertical bars would

have yielded before the complete closure of the gap. At this point, a plastic zone was associated with an extremely reduced stiffness which allowed for the high probability of the out of plane buckling occurred. Consequently, the Compression capacity of the wall was almost lost and to compensated by extending the compression zone into the unconfined length of the flange causing the complete crushing of the west flange (Figure 3.14).

(B) Failure of the East Flange (Distributed reinforcement)

When loading from O→E, the capacity of the wall dropped by approximately 35%, in comparison to the capacity of the wall along the previous cycles. The loading of the wall stopped at 1% SRSS drift in the E-F diagonal direction because of the full damage of the west flange. Loading in the E-F diagonal direction was alternated by loading in the G-H diagonal after the 1% SRSS drift. At 2.5% SRSS drift, this diagonal loading led to the compression crushing failure of the east flange (Figure 3.15).

(a) (b)

Figure 3.15 Failure of the East Flange TUC (Distributed Reinforcement) (Constantin & Beyer, 2016)

Concrete Compression failure (Crushing) a)Inside View, and b) Outside view. At SRSS drift = 1% Position H

(C) Relation between wall stability and the reinforcement layout

It was spotted from the test results that the east flange (distributed reinforcement) was less likely to be subjected to out of plane buckling than the west flange (concentrated reinforcement). Which suggests that the out of plane stability of the wall depends mainly on the maximum tensile strain value which activates the out of plane behavior. This value is inversely proportional to the vertical reinforcement ratio, this is why the west flange with concentrated reinforcement suffered from out of plane buckling.

(D) Crack Pattern

Crack Pattern in the web was similar to the web in TUA and TUB, while for the flanges the crack width and angles were different for the east flange and the west flange. The difference was mainly due to the different reinforcement layout. It was observed that for the concentrated reinforcements layout, the unconfined zone of the flanges had a crack width almost 40% larger than the distributed reinforcement layout, this led to more damage in the unconfined concrete of the west flange. Crack angles measured counterclockwise with the vertical were lower for the west in comparison with east flange, this was a result of higher force capacity in tension of the west flange.

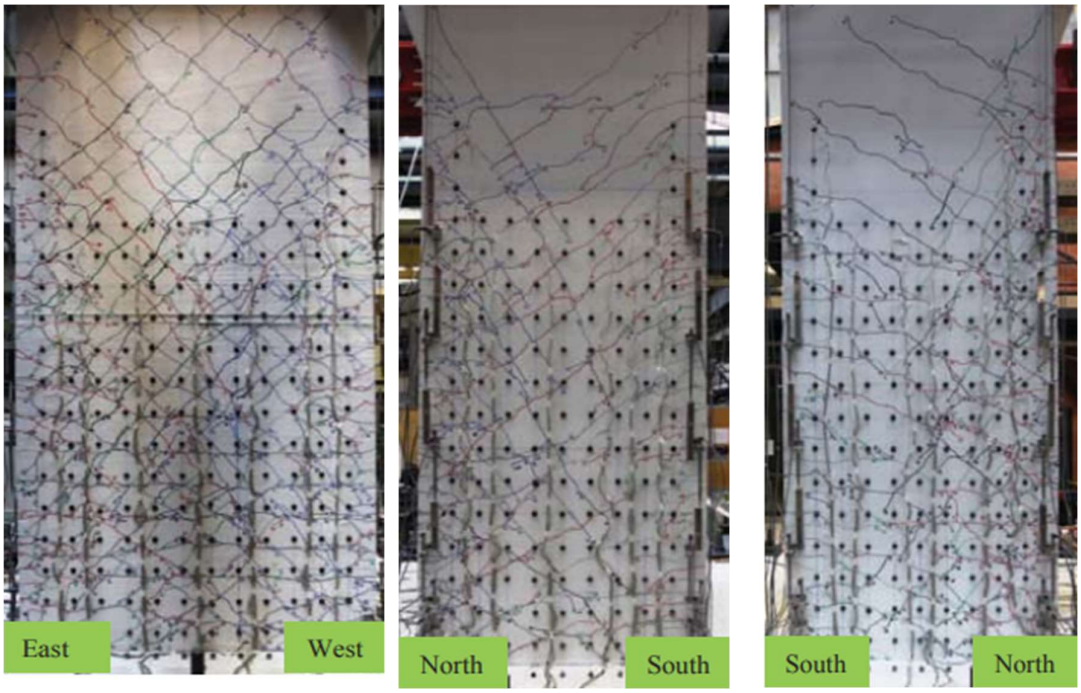

(a) Web

(b) West Flange (Concentrated Reinforcement)

(b) East Flange (Distributed Reinforcement)

Figure 3.16 Crack Pattern of TUC (Constantin & Beyer, 2016)

3.3.2. Hysteretic behavior

The division of the internal forces between the various elements in a U-shaped shear wall subjected to bi-directional loading is immensely complex and important to know as it affects the design procedures. Displacements, moments, and actuator force were calculated from the E-W and N-S actuators by combining the effects through SRSS combination rule through the equations.

$$M_{SRSS} = \sqrt{{M_{EW}}^2 + {M_{NS}}^2}.Sign(\Delta_{NS}) \quad \text{Eq. 3.1}$$

$$\Delta_{SRSS} = \sqrt{{\Delta_{EW}}^2 + {\Delta_{NS}}^2}.Sign(\Delta_{NS}) \quad \text{Eq. 3.2}$$

$$F_{SRSS} = \sqrt{{F_{EW}}^2 + {F_{NS}}^2}.Sign(\Delta_{NS}) \quad \text{Eq. 3.3}$$

The graphs show the hysteretic history of the E-W, N-S and diagonal directions for TUA and TUB but the sweep cycles were not considered in the graphs. While, for TUC as it is mainly loaded in the diagonal directions an additional diagonal direction was added to study the difference between the reinforcement layout of the two flanges (Figure 3.17 to Figure 3.22).

(A) E-W Cycles

For TUA and TUB, the force-deformation curve shows a symmetric hysteresis loops resembling hysteresis loops resulting from a symmetric planar wall loaded in a unidirectional cyclic loading.

(B) N-S Cycles

For TUA and TUB, the walls were loaded in line with the axis of symmetry of the wall which facilitated the force distribution between the two flanges equally, while the web carries a negligible amount of the force share. But during the test, the stiffness of each flange was different due to different crack pattern causing a change in the forces carried by each flange.

(C) Diagonal Cycles

For the Three tests units, the load transfer mechanism was very complicated in the diagonal loading for several considerations:

1. Incompatible stiffness of the flanges, as the stiffness of the compression flange is higher than the tension flange.
2. Limited zones for transferring the shear forces to the foundation at the base due to the open cracks at the base reducing the compression zone which transfer the shear.

3.3.2.1. TUA

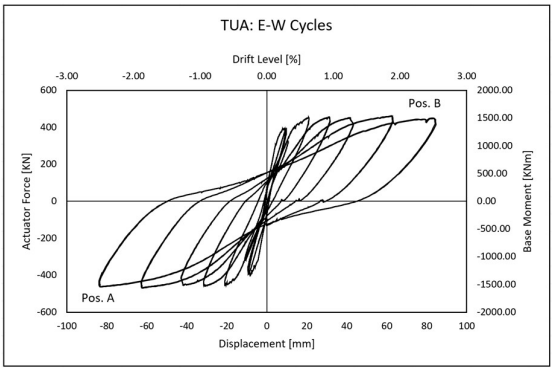

(a) E-W Direction

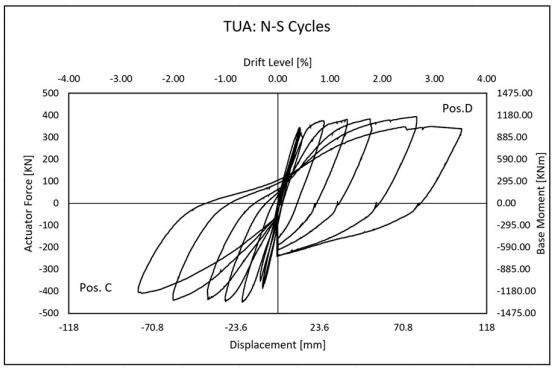

(b) N-S Direction

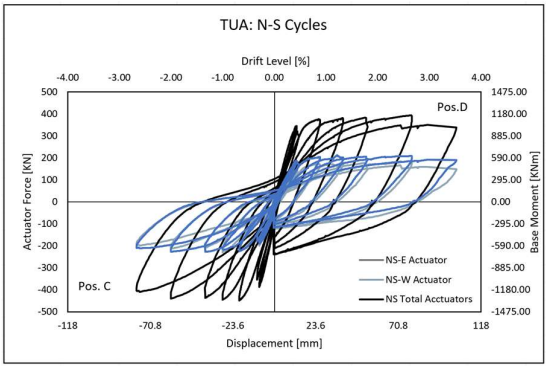

(c) N-S Direction Each Actuator

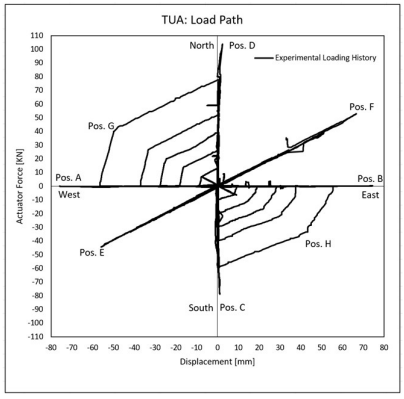

(d) Imposed Loading History

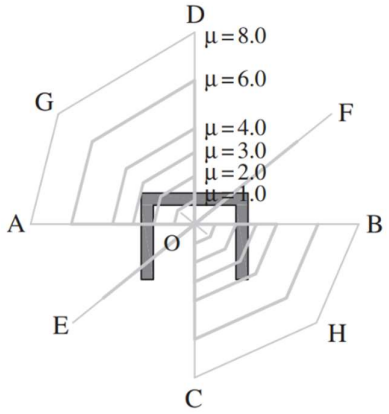

(e) Loading Directions

Figure 3.17 Force-Displacement Hysteresis for EW and NS for TUA (Beyer et al., 2008b)

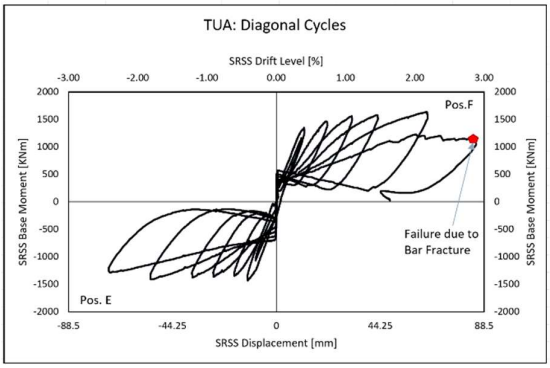

(a) Diagonal Direction

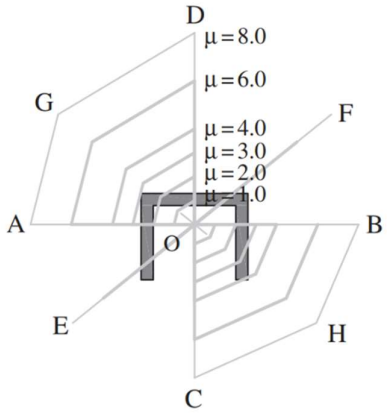

(b) Loading Directions

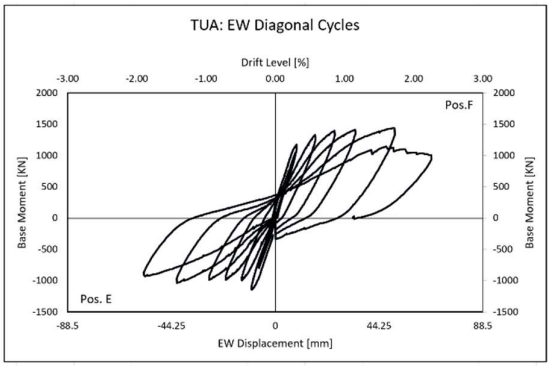

(c) E-W Diagonal cycle

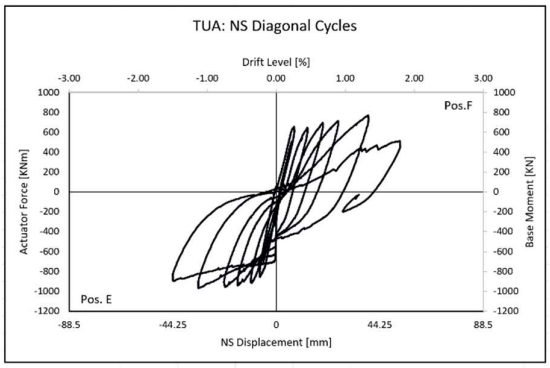

(d)NS Diagonal cycle

Figure 3.18 Force-Displacement Hysteresis for diagonal Cycles for TUA(Beyer et al., 2008b)

3.3.2.2. TUB

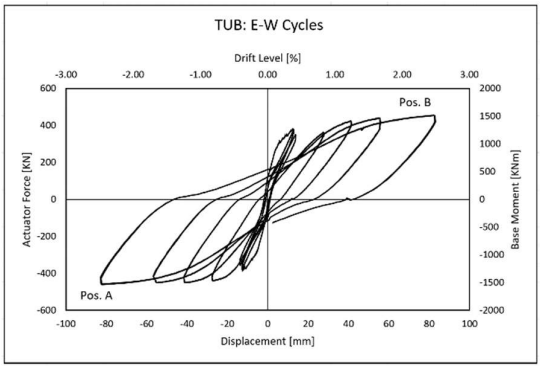

(a) E-W Direction

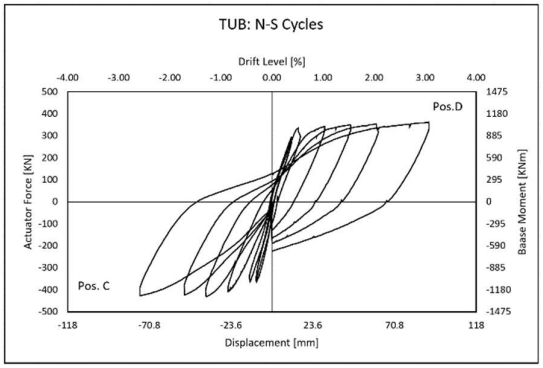

(b) N-S Direction

Figure 3.19 Force-Displacement Hysteresis for EW and NS for TUB(Beyer et al., 2008b)

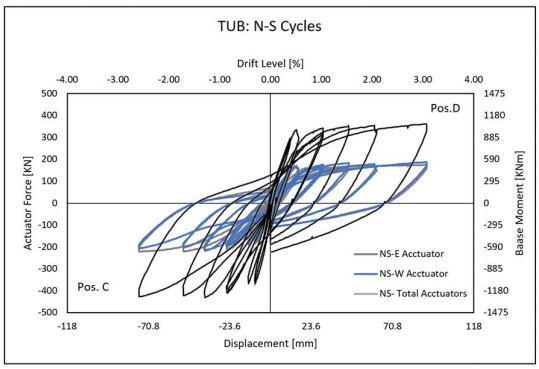

(c) N-S Direction Each Actuator

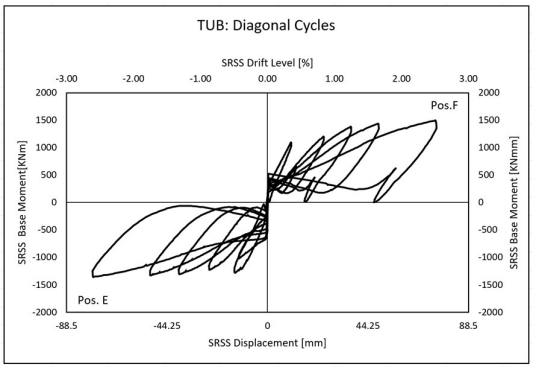

(d) Diagonal Direction

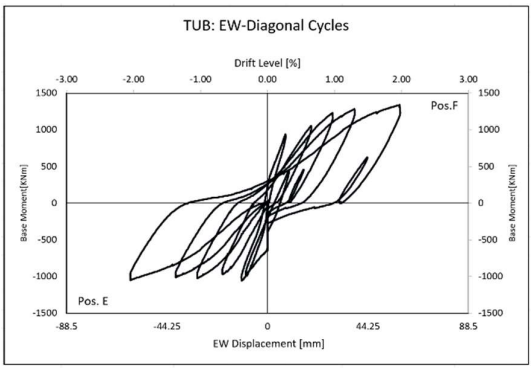

(e)EW Diagonal cycle

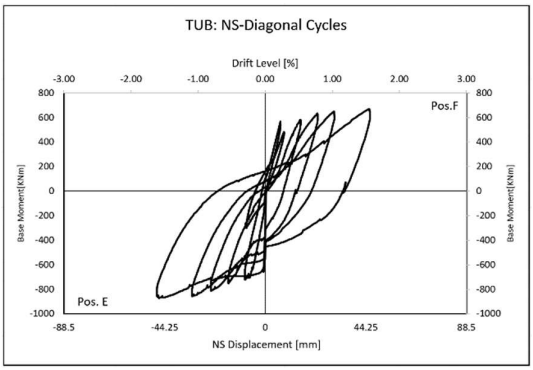

(f)NS Diagonal cycle

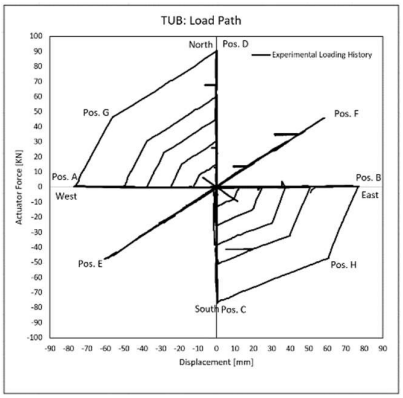

(g) Imposed Loading History

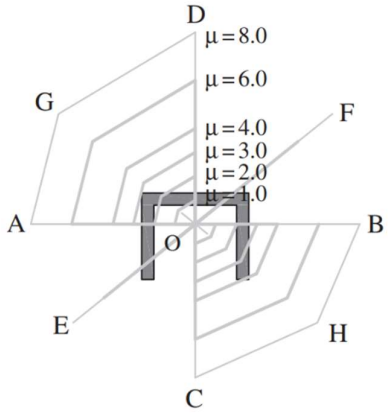

(h) Loading Directions

Figure 3.20 Force-Displacement Hysteresis for TUB(Beyer et al., 2008b)

3.3.2.3. TUC

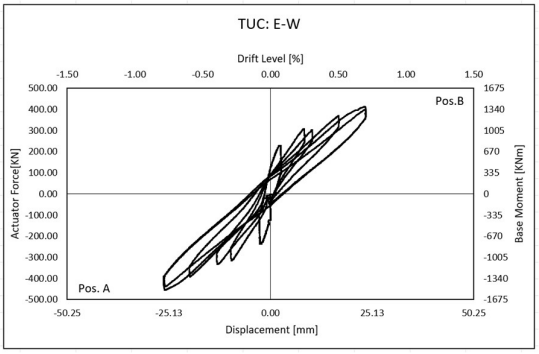

(a)E-W Direction

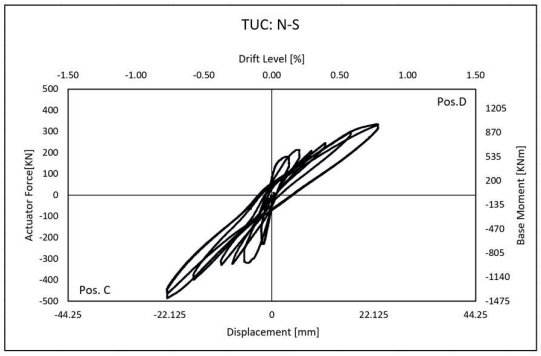

(b) N-S Direction

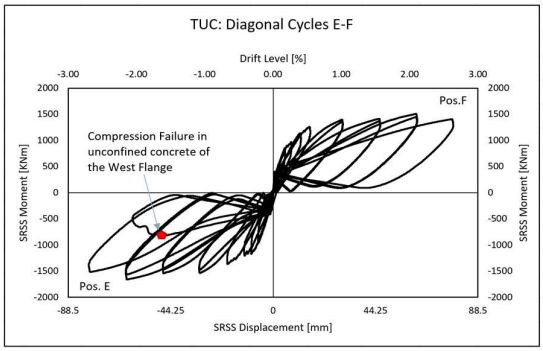

(c) E-F Diagonal Direction

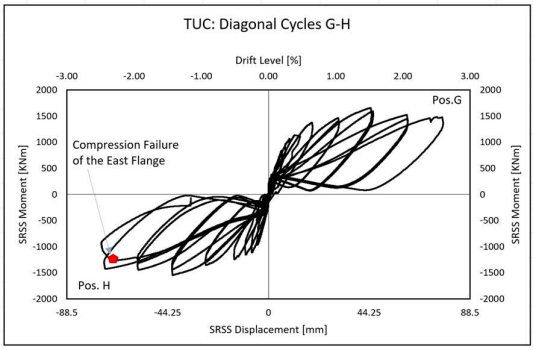

(d) G-H Diagonal Direction

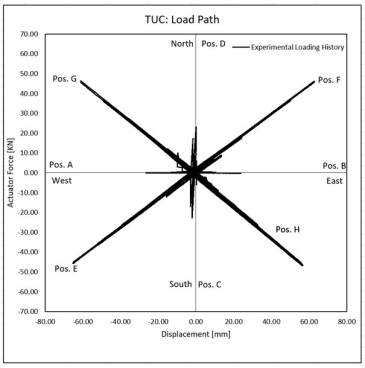

(e) Imposed Loading History

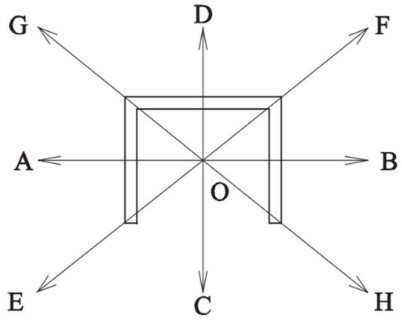

(f) Loading Directions

Figure 3.21 Force-Displacement Hysteresis for TUC(Constantin & Beyer, 2016)

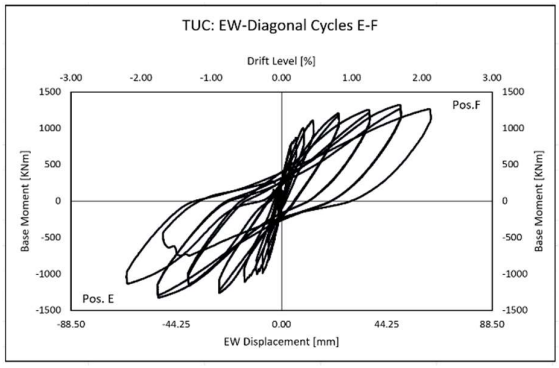

(a) EW Diagonal cycle position E-F

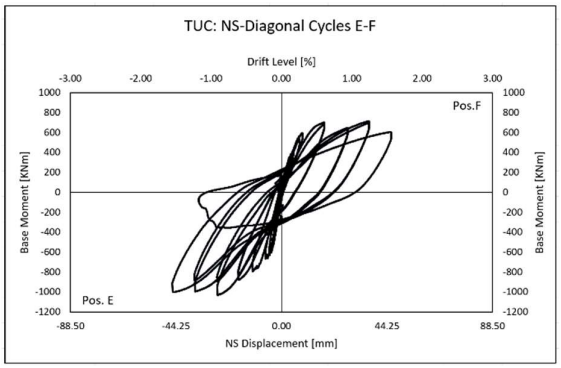

(b) NS Diagonal cycle position E-F

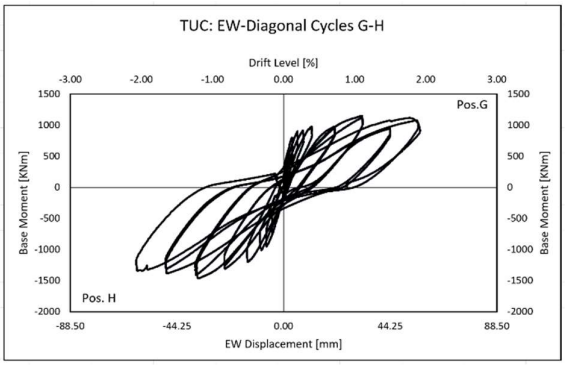

(c) EW Diagonal cycle position G-H

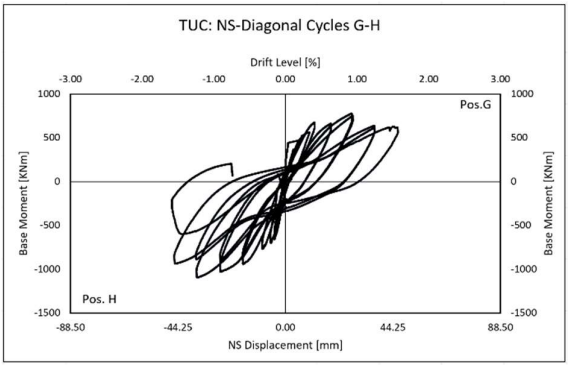

(d) NS Diagonal cycle position G-H

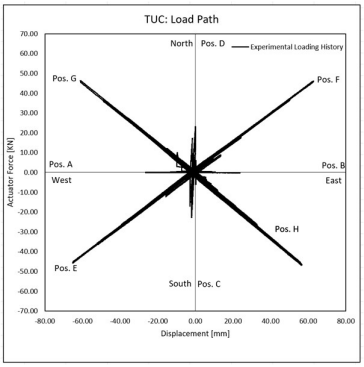

(e) Imposed Loading History

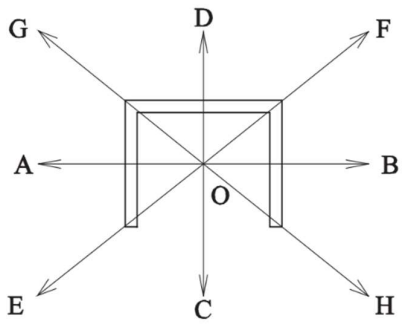

(f) Loading Directions

Figure 3.22 Force-Displacement Hysteresis for diagonal Cycles for TUC(Constantin & Beyer, 2016)

4 Numerical Modeling of non-planar walls

4.1. Scope and Objectives

This section focuses the attention on the non-linear modeling of the non-planar RC walls by using a macroscopic model element which is implemented into the structural analysis software OpenSees. So, the objective of this chapter is to develop a three-dimensional finite element model that presents non-linear analysis of non-planar RC walls under multi-directional loading and validate the numerical results with the experimental results.

4.2. Overview of OpenSees Software

OpenSees (Open system for Earthquake Engineering Simulation) is an opensource software framework developed by (Mazzoni et al., 2006) in the Pacific Earthquake Engineering Research Center (PEER) at the University of California, Berkeley. It is used by researchers and engineers to model and be able to analyze the behavior of different structural systems subjected to seismic loading protocols. It has a wide collection of finite elements, materials, numerical integration techniques and diverse types of analysis that opens the choices to the user based on the study.

4.3. Evolution of the MVLEM-3D element

A new three-dimensional beam-column formulation of the MVLEM (Multiple-Vertical-Line-Element) was developed and implemented by (Kolozvari et al., 2021) in efforts of increasing the accuracy of the analytical models for non-planar RC shear walls. The MVLEM-3D element is an extension of the original MVLEM element implemented by(Vulcano A., 1992) , (Orackal et al., 2004) & (Kolozvari et al., 2016).

4.3.1. MVLEM-2D Element

The original MVLEM element was a two-dimensional, two-node-element having six in-plane degrees of freedom located at the center nodes of the upper and lower rigid beams, each node has three degrees of freedom (ψ_i), two translation and one rotational as shown in (Figure 4.3). The RC wall cross section is implemented as a number (m)

vertical fibers modeling the concrete and reinforcement areas. Strains at each fiber are computed in relation to all the degrees of freedom and applying the plane section assumption for the top and bottom rigid beams. Relative rotation of the element is presumed to take place at the element centerline at a height of (c.h) from the bottom node where c is a variable ranging from 0 to 1, h is the height of the element (Figure 4.1).

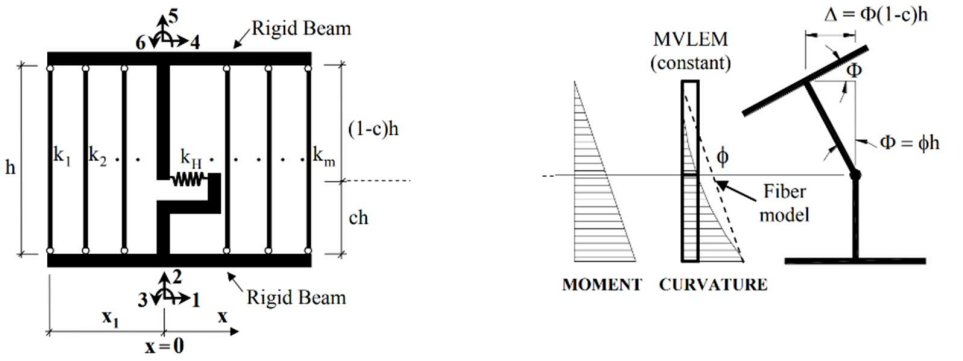

(a) Model element formulation

(b) Rotations and displacements

Figure 4.1 MVLEM element (Orackal et al., 2004)

Material models can be assigned to each fiber to model the hysteretic stress-strain behavior of the concrete and steel bars using uniaxial constitutive laws, regulating the flexural and axial behavior. Additionally, a horizontal spring is used to model the shear behavior at height (c.h) from the bottom of the element, a force-deformation relationship should be assigned to control the behavior of the spring. It is crucial to underline that the shear behavior is uncoupled from the flexural and axial behavior (Figure 4.2).

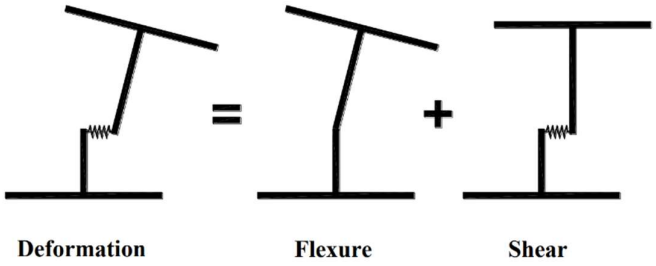

Figure 4.2 Uncloupling between Shear and Flexural Behavior(Orackal et al., 2004)

4.3.2. Upgrade from MVLEM-2D to MVLEM-3D

4.3.2.1. In-plane behavior of the Element

The upgrade comprised an increase in the number of nodes from two nodes at the center of rigid beams to four nodes at the ends of the two rigid beams, where each node has three degrees of freedom horizontal, vertical, and rotational degree of

freedom giving a total of twelve degrees of freedom(Δ_k) as shown in Figure 4.3. This upgrade was done using a geometric transformation matrix [C]

$$\{\Delta\}_{12\times1} = [C]_{12\times6} \times \{\psi\}_{6\times1}$$

Where [C] is defined as:

$$[C]_{12\times6} = \begin{bmatrix} [c_1]_{3\times3} & [0]_{3\times3} \\ [c_2]_{3\times3} & [0]_{3\times3} \\ [0]_{3\times3} & [c_3]_{3\times3} \\ [0]_{3\times3} & [c_4]_{3\times3} \end{bmatrix}_{12\times6}$$

Where $[c_i]$ corresponds to the rigid transformation of each of the four nodes as:

$$[c_i] = \begin{bmatrix} 1 & 0 & 0 \\ 0 & 1 & x \\ 0 & 0 & 1 \end{bmatrix}_{3\times3}$$

Where X= L_w/2 characterizes the horizontal distance of each corner of the element from the centerline, L_w is the wall length.

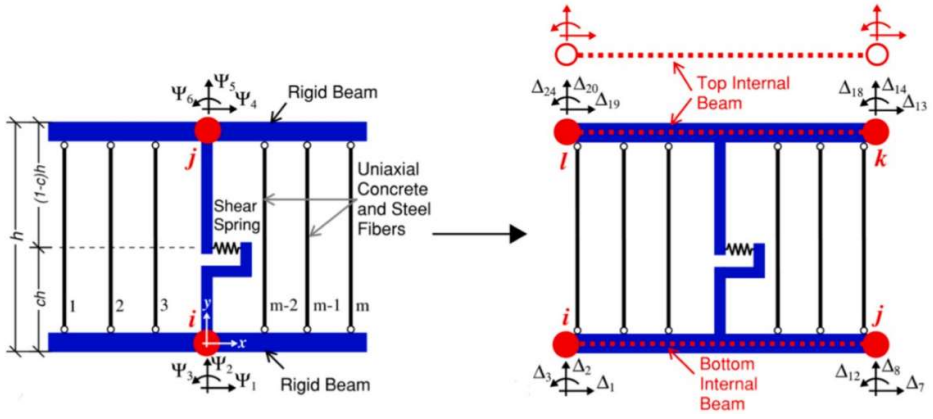

Figure 4.3 Transformation of MVLEM from 2-node, 6-DOFs formulation to 4-node, 12-DOFs formulation.

4.3.2.2. Out-of-plane behavior of the Element

An additional four-node Kirchhoff plate finite element formulation was added to the original MVLEM to take into consideration the out-of-plane behavior, which follows four basic assumptions:

1. Homogenous, linear elastic material behavior.
2. The thickness of the plate is constant and comparably small to other dimensions.
3. Out-of-plane deformations are limited compared to in-plane deformations.
4. Effects of transverse shear and shear strain energy are ignored.

The plate element has three degrees of freedom at each of its four nodes, two rotations plus one translation resulting in a total of twelve out-of-plane degrees of freedom (Δ_k) as shown in (figure 4.4b). It is important to note that the out of place behavior is decoupled from the in-plane behavior.

4.3.2.3. Shear behavior

The shear behavior is the same as the original MVLEM formulation with presence of the shear spring at a specific height (c.h).

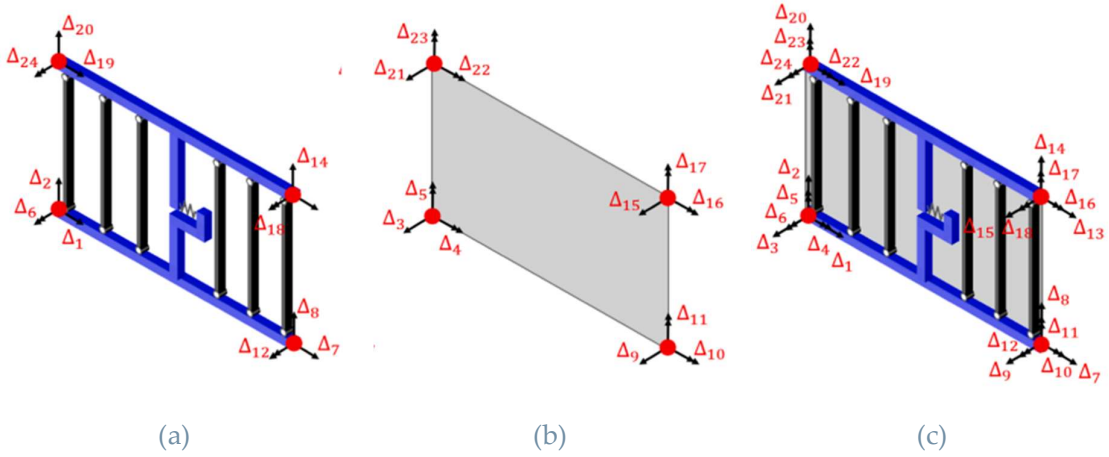

(a) (b) (c)

Figure 4.4 Formulation of MVLEM-3D (Kolozvari et al., 2021)

a) element in plane bending behavior represented by four-node MVLEM formulation, b) element out of plane behavior represented by the four-node Kirchhoff plate and, c) combined in-plane and out-of-plane behavior.

4.3.3. Implementation of MVLEM-3D element in OpenSees

The element is name as "*MVLEM_3D*" in the non-linear analysis software openSees (Mazzoni et al., 2006), which can operate in three-dimensional domain. The input parameters are represented in Table 4.1 mentioned by (Kolozvari et al., 2021)

User input format	element MVLEM_3D eleTag iNode jNode kNode lNode m -thick {Thicknesses} -width {Widths} -rho {Reinforcing_ratios} -matConcrete {Concrete_tags} -matSteel {Steel_tags} -matShear {Shear_tag} <-CoR c> <-thickMod tMod> <-Poisson Nu> <-Density Dens>	
Description of input parameters	eleTag	Unique element tag
	iNode jNode kNode lNode	Tags of element nodes defined in counterclockwise direction
	m	Number of element macro-fibers
	{Thicknesses}	Array of m macro-fiber thicknesses
	{Widths}	Array of m macro-fiber widths
	{Reinforcing ratios}	Array of m reinforcing ratios corresponding to macro-fibers
	{Concrete_tags}	Array of m uniaxial Material tags for concrete
	{Steel_tags}	Array of m uniaxial Material tags for steel
	{Shear_tag}	Tag of uniaxial Material for shear material
	c	Location of center of rotation from the base (optional; default = 0.4 (recommended))
	tMod	Thickness modifier for out-of-plane bending behavior (optional; default = 0.63, which is equivalent to 25% of uncracked stiffness)
	Nu	Poisson ratio for out-of-plane bending behavior (optional; default = 0.25)
	Dens	Element density (optional; default = 0.0)

Table 4.1 OpenSees user input for MVLEM_3D element

4.4. Description of Modeling Approach

This section is focusing the attention on the modeling of the U-shaped walls which were subjected to multidirectional testing protocols TUA, TUB by (Beyer et al., 2008b) and TUC by (Constantin & Beyer, 2016) In more general words, the modeling approaches that will be discussed in the following sections could be applied on any non-planar walls within the OpenSees framework.

4.4.1. Constitutive Models and Material Model Calibration

A detailed brief is given on the uniaxial constitutive models used for concrete, reinforcing steel, and wall shear response in the modeling of the non-planar walls. Moreover, the parameters which were used to calibrate the material model are stated in detail. When dealing with MVLEM-3D element, it is possible to apply any uniaxial constitutive model in the OpenSees library.

4.4.1.1. Concrete Constitutive Behavior

The uniaxial material mode "Concrete02"(Yassin, 1994) was used to reflect the hysteretic behavior of concrete within the longitudinal fibers of the MVLEM 3-D. Simplicity and optimal computational efficiency were the reasons behind the choice of the material model Concrete02. It can capture some important aspects of concrete behavior under cyclic loading such as tension stiffening and hysteretic stiffness degradation.

(Kent & Park, 1971) and (Scott et al., 1982)relationships were the baseline for building the compression envelope curve, where the loading phase adheres to a quadratic relation while the post-peak loading phase is considered as linear relation until it reaches a constant residual stress capacity. For tension envelope curve, the loading phase had a constant slope equivalent to the concrete tangent modulus until it reaches the cracking stress then it follows a decreasing slope till it reaches the zero stress.

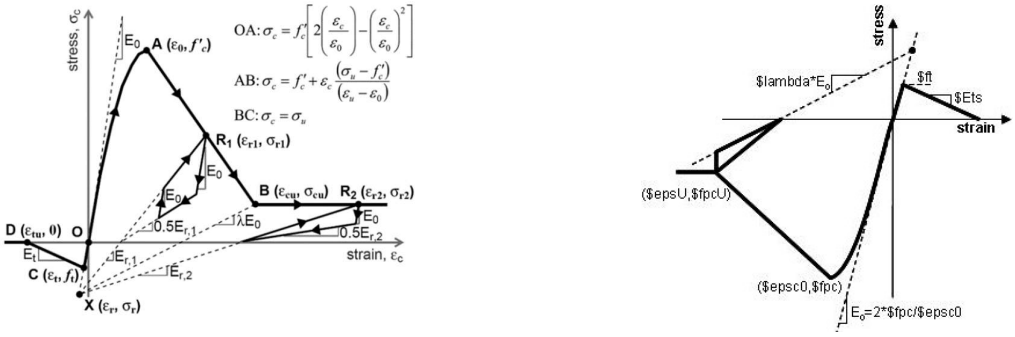

Figure 4.5 Concrete Material Model

a)Concrete model by (Kent & Park, 1971) and, b)Concrete02 implementation in OpenSees

For the calibration of the unconfined concrete properties on the concrete02 material model, the loading envelope for compression was based on maximum compressive stress - strain values obtained from a cylindrical specimen that were reported in the material reports attached with the test documents. However, for the confined concrete the loading envelope for compression was derived by the confinement model by (Mander et al., 1988). After reaching the peak value of compressive stress, the path follows a negative linear slope reaching a value residual stress equals to zero for

unconfined concrete. While for confined concrete equals to 20% of peak compressive strength based on the recommendation by (Saatcioglu & Razvi, 1992). For the tensile strength of concrete, it was evaluated as $f_t = 0.31\sqrt{f_c'}$ [MPa] in accordance with the recommendation by (Belarbi & Hsu, 1994). To consider the tension stiffening effects on the stress-strain behavior, the slope of the post cracking model envelope in tension was taken as 5% from the initial tangent modulus of concrete which was recommended by (Yassin, 1994).The material testing of a number of concrete cylinders are shown in Figure 4.6 also showing the concrete strength of the confined and the unconfined zones that are calibrated in the model. The experimental materials testing data were attached with the test results supplied by prof. Beyer.

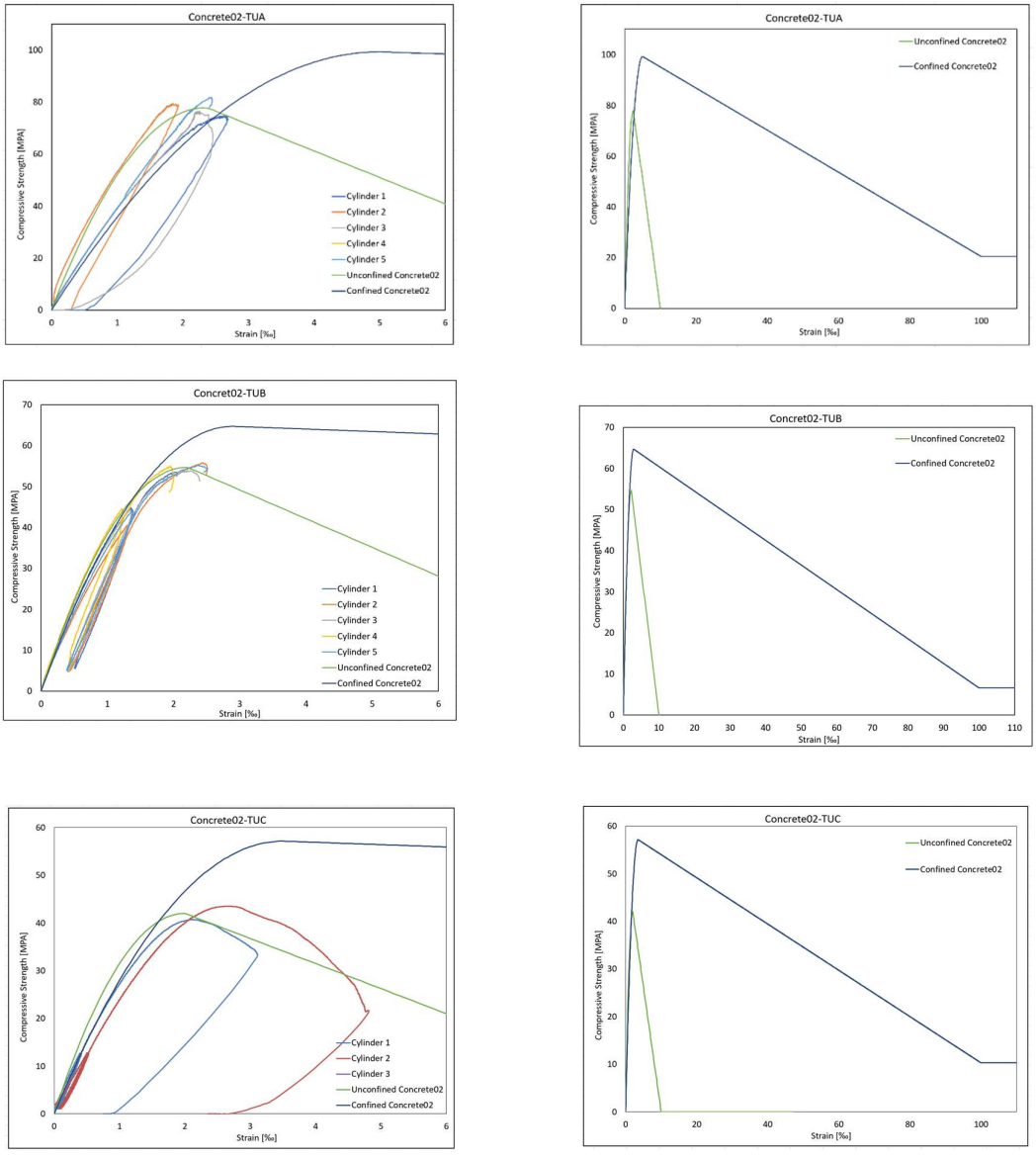

Figure 4.6 Concrete02 Calibration

User input format	uniaxialMaterial Concrete02 matTag fpc epsc0 fpcu epsU lambda ft Ets	
Description of input parameters	matTag	integer tag identifying material
	fpc	concrete compressive strength at 28 days (compression is negative). The values for the unconfined and confined concrete TUA: unconfined fpc=77.9MPa, confined fpc=99.305MPa TUB: unconfined fpc=54.7MPa, confined fpc=71.325MPa TUC: unconfined fpc=42.0MPa, confined fpc=57.140MPa
	epsc0	concrete strain at maximum strength the unconfined and confined concrete TUA epsc0=0.00236, ecc= 0.005 TUB epsc0=0.00221, ecc= 0.0045 TUC epsc0=0.002, ecc= 0.0054
	fpcu	concrete crushing strength;0 for unconfined concrete TUA 15.58MPa, TUB 10.94MPa, TUC 8.40MPa
	epsU	concrete strain at crushing strength epsU= -0.01 for the unconfined, -0.1 for the confined
	lambda	ratio between unloading slope at epscu and initial slope TUA= 0.08, 0.08 TUB= 0.08, 0.069 TUC= 0.08, 0.069
	ft	tensile strength TUA=2.736MPa TUB= 2.29 MPa TUC= 2.00MPa
	Ets	tension softening stiffness (absolute value) (slope of the linear tension softening branch TUA=1850MPa TUB= 1675MPa TUC= 1580MPa

Table 4.2 OpenSees user input for Concrete02

4.4.1.2. Reinforcing Steel Constitutive Behavior

The reinforcing steel positioned in the longitudinal fibers of the MVLEM-3D element is simulated according to the cyclic material model by (Menegotto & Pinto, 1973) which was extended by (Fllippou et al., 1983). This material model has a bi-linear stress strain relationship for monotonic loading representing the elastic (E_0) and plastic branches ($b.E_0$) where b is the strain hardening ratio, The shift between the elastic and plastic linear lines is defined with a curve of a curvature (R_0). During cyclic loading, the unloading and reloading envelope happen at the same slope (E_0) with decreasing shift characterized by a curvature depending on the applied strain history which captures the Bauschinger effect.

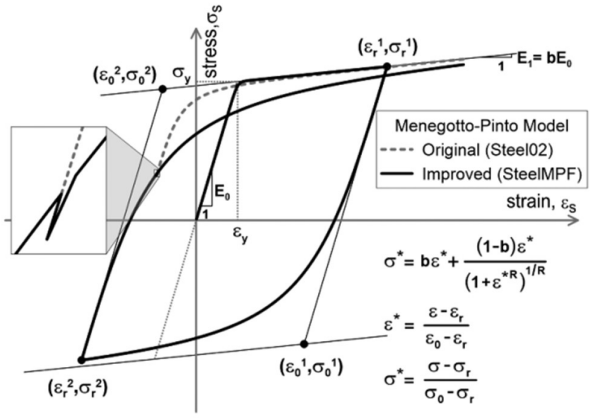

Figure 4.7 Steel Material Model

SteelMPF (Kolozvari et al., 2018) was used in modeling the reinforcement steel since it is an improvement to the older Steel02. The main improvements were solving i) the stress overshooting issue after unloading and reloading, enhancing steel stresses predictions. ii) degradation of the cyclic curvature parameter (R) was added to increase the accuracy of wall lateral yield capacity (Kolozvari et al., 2018).

For the calibration of the SteelMPF material model, yielding stress – strain, and hardening ratio were chosen based on the tension tests attached with the test documents, where the strain hardening ratio was the ration between the (E_0) and the line joining the yield and ultimate stress. Modulus of elasticity (E_0) was assumed to be constant 200,000 MPa for all bar diameters and for all the test units. Cyclic stiffness degradation properties of the steel hysteretic behavior were defined by the following parameters (R_0) = 20 ,(CR_1) = 0.925 ,and (CR_2) = 0.15 following the suggestions of (Menegotto & Pinto, 1973).

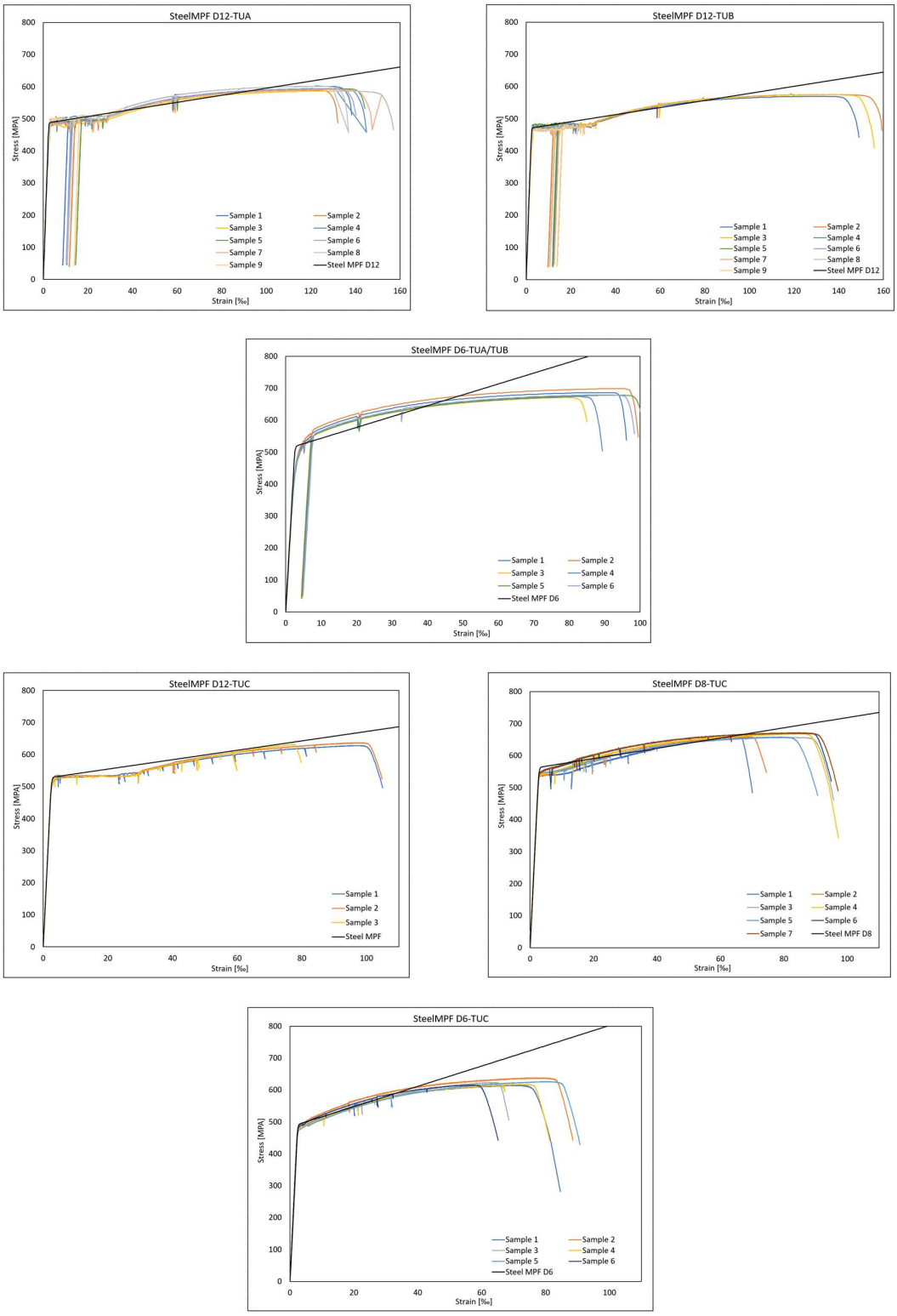

Figure 4.8 SteelMPF Calibration for TUA, TUB and TUC

User input format	uniaxialMaterial SteelMPF mattag fyp fyn E0 bp bn R0 cR1 cR2 <a1 a2 a3 a4>	
Description of input parameters	mattag	Unique uniaxialMaterial tag
	fyp	Yield strength in tension (positive loading direction) TUA; D6:518MPa, D12:488MPa TUB; D6:518MPa, D12:471MPa TUC; D6 492MPa, D8:563MPa, D12:529MPa
	fyn	Yield strength in compression (negative loading direction);same values of fyp
	E0	Initial tangent modulus; 200,000MPa
	bp	Strain hardening ratio in tension (positive loading direction); TUA and TUB; D6:0.017, D12:0.0055 TUC; D6 0.0159, D8:0.00417, D12 0.00734
	bn	Strain hardening ratio in compression (negative loading direction); same values of bp
	R0	Initial value of the curvature parameter R (R0 = 20 recommended)
	cR1	Curvature degradation parameter (a1 = 0.925 recommended)
	cR2	Curvature degradation parameter (a2 = 0.15 or 0.0015 recommended)
	a1	Isotropic hardening in compression parameter (optional, default = 0.0). Shifts compression yield envelope by a proportion of compressive yield strength after a maximum plastic tensile strain of a2(fyp/E0)
	a2	Isotropic hardening in compression parameter (optional, default = 1.0). See explanation of a1.
	a3	Isotropic hardening in tension parameter (optional, default = 0.0). Shifts tension yield envelope by a proportion of tensile yield strength after a maximum plastic compressive strain of a3(fyn/E0).
	a4	Isotropic hardening in tension parameter (optional, default = 1.0). See explanation of a3.

Table 4.3 OpenSees user input for SteelMPF

4.4.1.3. Shear behavior

The in-plane shear behavior of the MVLEM-3D element is presented by the shear spring which shows the decoupling between the flexural and the shear response. A force-deformation relation should be defined to be assigned to this shear spring, there were many admissible alternatives to choose from, such as a linear elastic model with a defined effective shear stiffness, or a multilinear curve. A study was done by (Kolozvari & Wallace, 2016) showed that utilizing an elasto-plastic shear force-deformation relationship produced an unrealistic behavior as the overall deformation of the wall becomes dominated by shear deformations just after reaching the shear force capacity of the element. For this reason, the choice for the shear force-deformation was linear elastic with an effective shear stiffness which is also the most common practical approach.

As for the value of the effective shear stiffness, there are wide range of values recommended by design provisions and researches. 0.5G is recommended by (Akelyan & Brandow, 2020; PEER, 2017), while some analytical studies done by (Gogus Arup, 2010) on slender walls showed that an effective shear modulus of 0.025G is the most relevant after shear cracking. All the previous values for effective shear stiffness were computed relying on unidirectional loading of planar walls which might be not suitable for multidirectional loading of non-planar shear walls.

Shear deformation measured from the test done by (Beyer et al., 2008b) for U-shaped shear walls was hugely affected by the loading direction, where shear deformation was larger in the zones with a tension (flexural + axial) resultant stress. It is worth mentioning that the shear deformations in the tests were much larger than that of the planar walls, resulting in a lower effective shear stiffness. Taking all the above studies into consideration, 0.025G was chosen to represent the effective shear stiffness as it is also recommended by (Kolozvari et al., 2021) to represent the elastic shear stiffness in the MVLEM-3D elements for modeling non-planar walls.

4.4.2. Geometry Discretization

(STKO by ASDEA, 2021) " Sceintific Tool Kit for OpenSees" software developed by ASDEA Software Technology was used as a pre and post processor of the geometry and results. The cross-section geometry of the wall was divided into three separate elements: two flanges and a web. The geometry of the model was defined by three MVLEM 3-D elements where each MVLEM 3-D represents each element separately. The coordinates of the geometry in space were defined giving the C-shaped wall model. The height of the MVLEM3-D element (h=3.49m) was chosen to be similar to the length of the LVDTs which was inserted to measure the strains at the base of the wall in order to have a fair comparison between the test results and the numerical model results. Each MVLEM 3-D element is divided into multiple uniaxial fibers according to the reinforcement distribution across the wall geometry. The width of the

fibers and the number of fibers per each element (m) of TUA, TUB and TUC that are used in the modelling phase are shown in Figure 4.9. Since the longitudinal reinforcement was distributed in a uniform manner along the boundary and the webs of the fibers, so the ratio of the reinforcement was easily calculated by considering the area of longitudinal steel bars and the concrete in each fiber. For TUA, the reinforcement ratio of the flange of the boundary element at the flange tip, at the corner boundary element, outside the boundary element and the web were 0.02345, 0.00942, 0.00206 and 0.00201 respectively. While TUB, the reinforcement ratio of the flange for the boundary element at the flange tip, at the corner boundary element, outside the boundary element and the web were 0.02673, 0.002262, 0.002827and 0.002976 respectively. Since the reinforcement layout of the east flange and west flange of TUC was different so, the reinforcement ratio of the east flange of the boundary element at the flange tip, at the corner boundary element and outside the boundary element were 0.0146, 0.0161 and 0.0084 respectively, while the west flange 0.0267,0.0126, 0.0028 respectively. The ratios of the web reinforcement were 0.0094 outside the corner zone and 0.0134 in the corner boundary zone. The connection of the wall specimens with the foundation was considered pinned for the three test units. On the contrary, the top of wall was restrained from twisting through any multidirectional loading protocol.

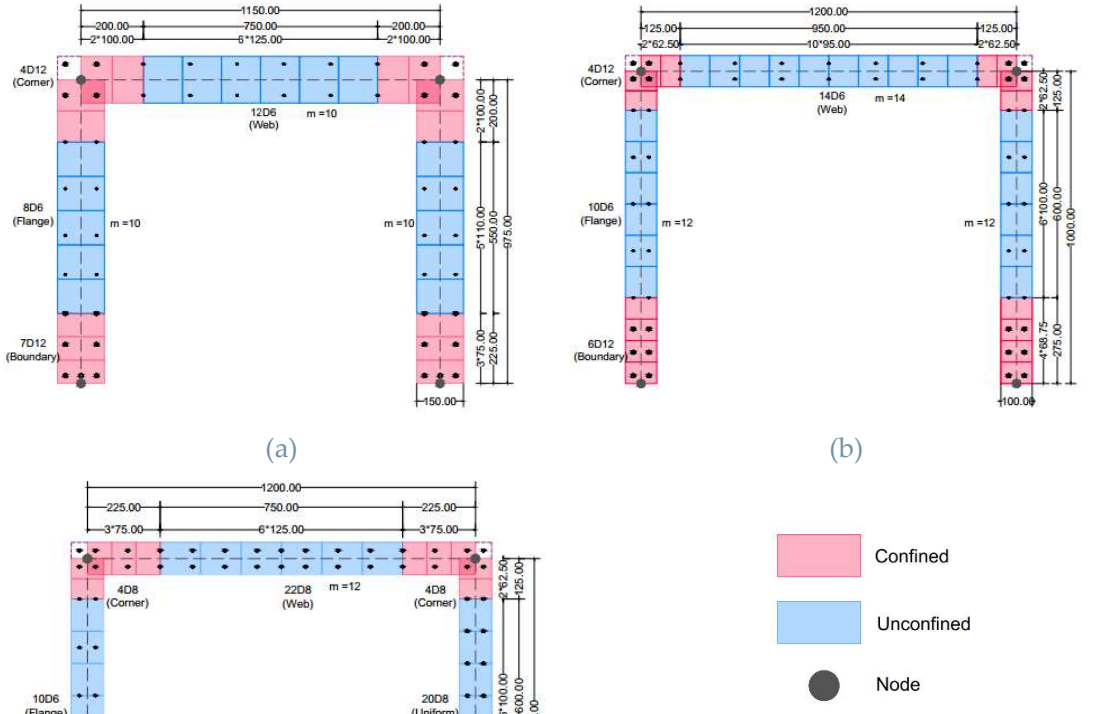

Figure 4.9 Model Discretization for a) TUA, b) TUB and c) TUC

The segments of the wall were connected with kinematic constraints that ensure the compatibility of only displacements in X, Y and Z directions. Each wall segment is under a plane section hypothesis which is the formulation that the MVLEM 3-D element is based on. This is the concept of Vlasov hypotheses when a common node shares the same displacement.

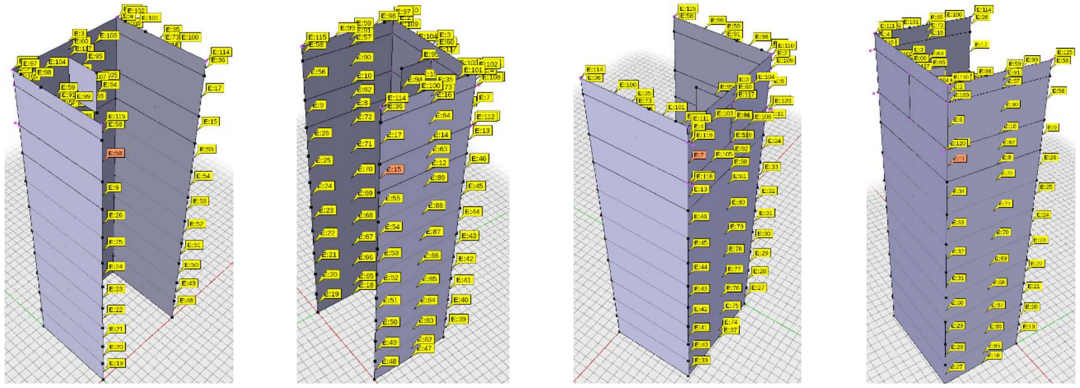

Figure 4.10 3D view with Element ID TUA

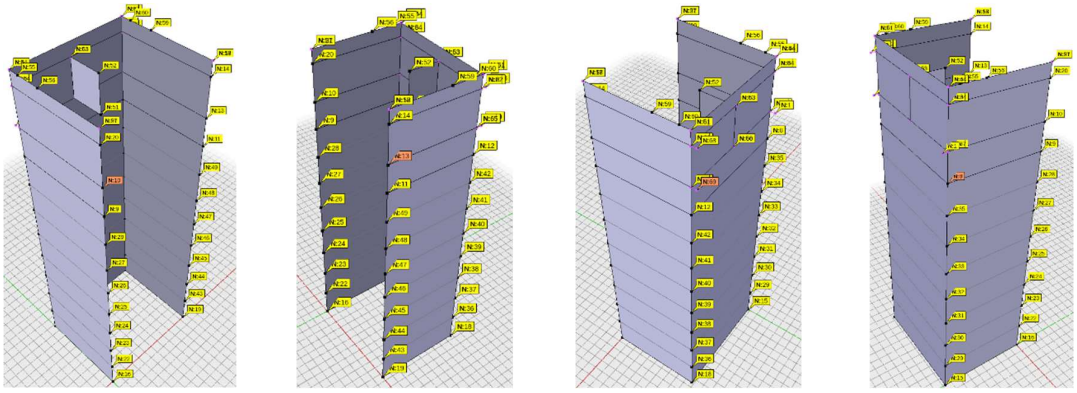

Figure 4.11 3D view with Node ID TUA

4.4.3. Load Application

The specimens were tested under a constant axial load applied at the top of the wall. The values of the load were applied similar to the values given in the test document in order to comply with the setting up of the test. In the experimental test, the axial load was applied through a beam supported on the top of the wall which was simulated in the numerical model by four-node-concentrated load located at the exact position of the supports of the beam (Figure 4.10).

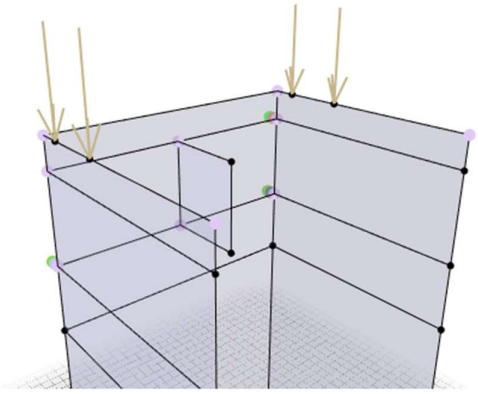

Figure 4.12 Axial Load Application

In addition to the cyclic lateral loading protocol that was applied to each of the specimens. A force-controlled analyses was chosen to allow the numerical models to reach the values of multidirectional loading history applied during the test, by which the load was applied at the position of the actuators. Figure 4.11 shows the numerical loading histories in comparison to the experimental loading histories. Analysis steps were carried out for each loading sequence. By which, the loading sequence could be for example from O to A and another sequence is from A to O. where each sequence consists of a 100 timestep.

The analysis consists of two stage: First stage was the gravity loading and the second stage was the cyclic loading. For the collection of the output results, a recorder was set to capture nodal results (Displacements) from a chosen control node corresponds to the node where the experimental data were collected, and reactions where captured at the base. Moreover, fiber strains at the base of the wall were recorded through gauss point results.

For the non-linear analyses of the wall units, to construct a solution algorithm, Krylov-Newton algorithm was chosen which uses a modified Newton method with Krylov subspace accelerator which determines the steps taken to solve the non-linear equations and accelerates the convergance (OpenSees command *Krylov-Newton*). The convergence test that was selected as the "Norm Displacement increment" test (OpenSees command test *NormDispIncr*) which determines if the convergence is

reached or not. So, Convergence is only maintained if the displacement increment is less than the error tolerance chosen, where the error tolerance was set to 10^{-5}.

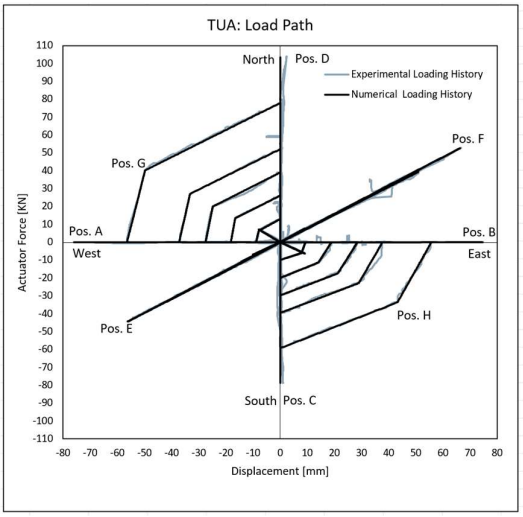

(a)TUA

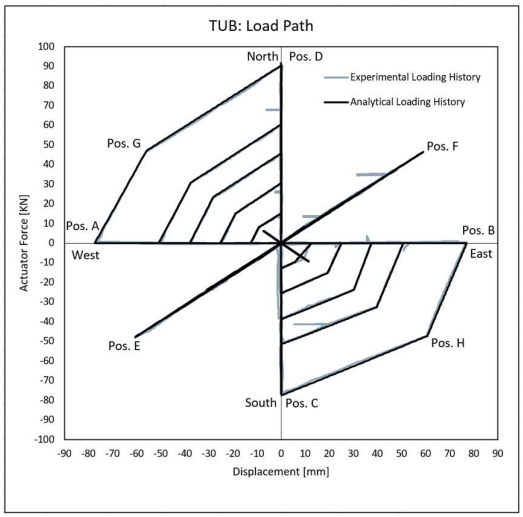

(b)TUB

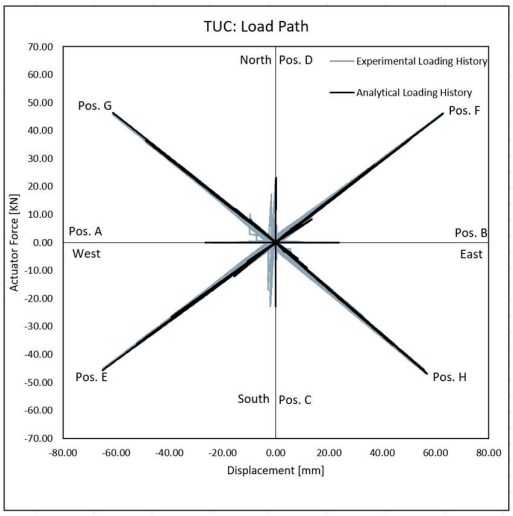

(c)TUC

Figure 4.13 Analytical Vs Experimental Loading History at h = 2.95m

5 Validation of the numerical models for U-shaped walls

This section focuses on the validation of the numerical model results in terms of global response (load-deformation) and local response in terms of strains at the base of the walls with the experimental results of the wall tested under multi-directional lateral loading. A comparison was made between the experimental and numerical results of the lateral force applied at the locations of the actuators and the peak deformation at the top of the test units in the main loading direction of each test i.e. (E-W, N-S, and diagonal directions) reported from Figure 5.1 to Figure 5.4. All the error percentages were computed based on the peak lateral forces in the experimental and numerical results.

5.1. TUA and TUB

For the loading cycles in the E-W direction the model showed good accuracy in capturing the lateral load capacity of the two tests units with an average error of 12%. Moreover, for the loading of TUA in the N-S direction in position D (web in compression) an overestimation of less than 5% error was observed. While, for TUB it shows an almost negligible error of 1%. By loading in the opposite direction position C (Position C) a similar overestimation was observed of approximately 18%.

For the loading in the diagonal direction, the numerical model exaggerated the capacity of the wall for TUA and TUB by an average error of 53% in position E (west flange boundary element in compression), while by reversing the loading direction to be in position F (northeast corner in compression) error was reduced to be around 20%. The reason behind the overestimations in the lateral load carrying capacity in the diagonal direction is the assumption of the plane section hypothesis which is assumed in the MVLEM-3D formulation, leading to an increase of the length in tension and the value of tensile strains of the flanges consequently increasing the capacity of the wall.

With respect to the shape of the hysteresis graph, the initial loading stiffens of the wall was in good agreement with the experimental results in loading in all directions. While, for the unloading stiffness an overestimation was noted from the graphs. Moreover, the general shape of the cyclic loops was well captured in comparison to the experimental load-displacement response.

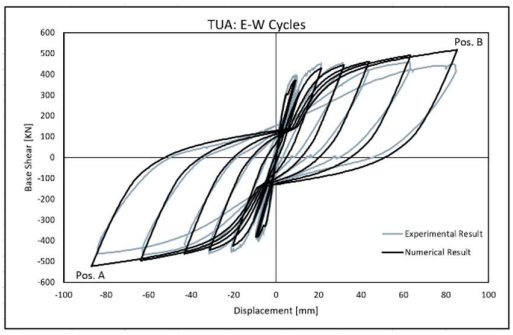

(a) E-W Direction-TUA

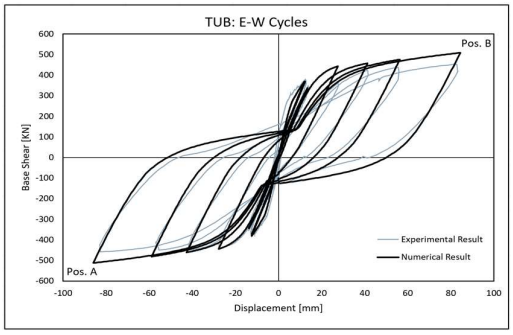

(b) E-W Direction-TUB

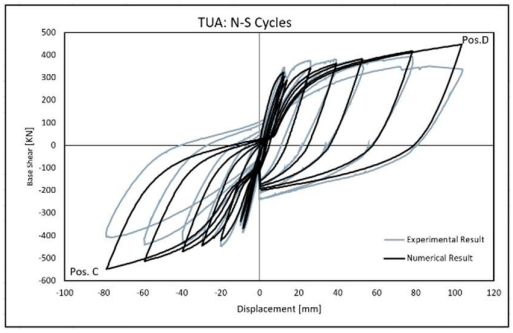

(c) N-S Direction-TUA

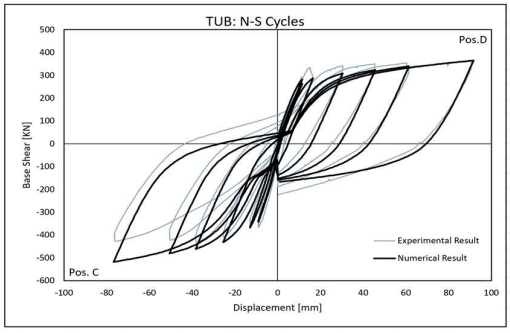

(d) N-S Direction-TUB

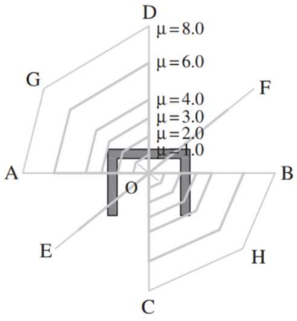

(f) Loading Direction-TUA and TUB

Figure 5.1 Comparison of Experimental and Numerical Force-Deformation Relationship for TUA and TUB

Experimental Result

Numerical Result

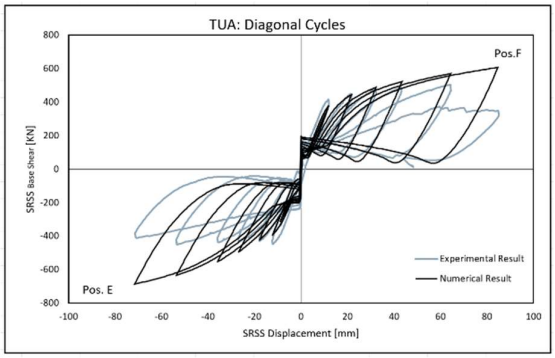

(a) Diagonal Direction-TUA

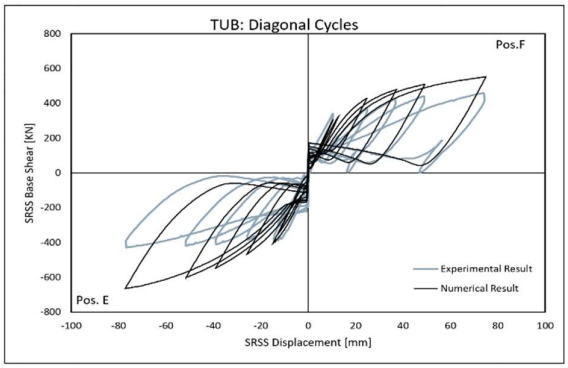

(b) Diagonal Direction-TUB

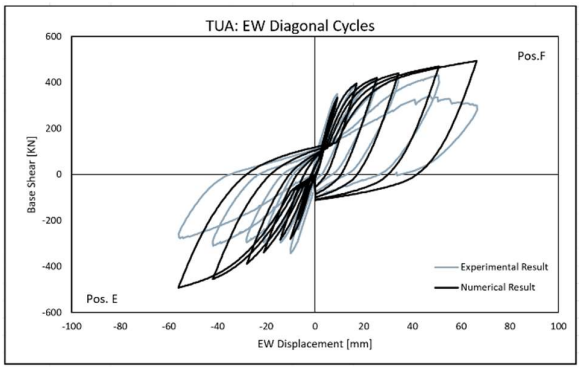

(c) E-W Diagonal cycle for TUA

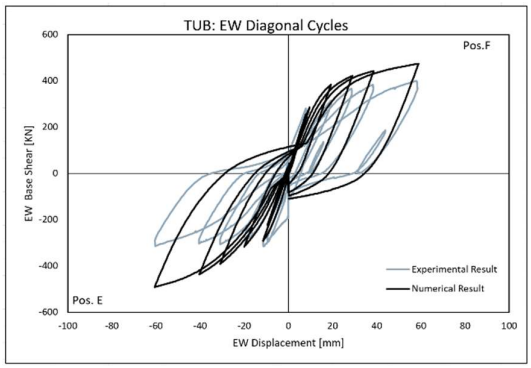

(d) E-W Diagonal Direction for TUB

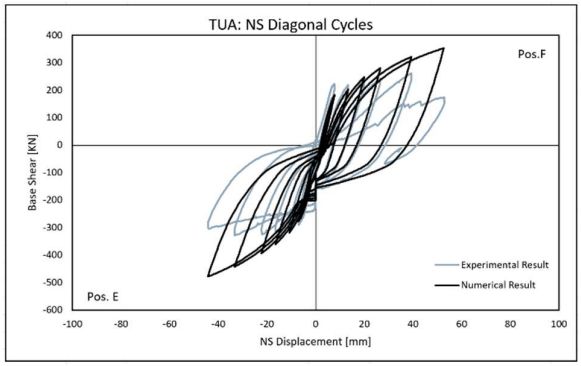

(e) N-S Diagonal Direction for TUA

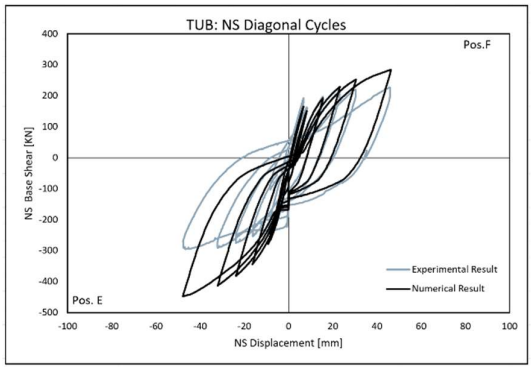

(f) N-S Diagonal Direction for TUB

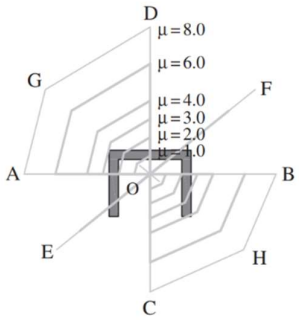

(g) Loading Direction-TUA and TUB

Figure 5.2 Comparison of Experimental and Numerical Force-Deformation Relationship for the diagonal cycles TUA and TUB

Experimental Result

Numerical Result

TUA		Imposed Displacement [mm]			Base Shear [KN]		
		Numerical Result	Experimental Result	Error	Numerical Result	Experimental Result	Error
E-W Cycles	Maximum (Position B)	74.60	74.37	0.31%	518.23	459.57	12.77%
	Minimum (Position A)	-75.97	-75.78	0.26%	-521.72	-467.13	11.69%
N-S Cycles	Maximum (Position D)	103,59	103,96	0,36%	447,43	459,57	2,64%
	Minimum (Position C)	-78,55	-78,75	0,25%	-548,31	-467,13	17,38%
Diagonal Cycles E-F	Maximum (Position F)	84,78	85,11	0,40%	606,92	503,58	20,52%
	Minimum (Position E)	-71,59	-71,38	0,30%	-685,33	-450,01	52,29%

Table 5.1 Comparison Between Numerical and Experimental Results TUA

TUB		Imposed Displacement [mm]			Base Shear [KN]		
		Numerical Result	Experimental Result	Error	Numerical Result	Experimental Result	Error
E-W Cycles	Maximum (Position B)	76,95	76,95	0,0%	509,134	453,81	12,19%
	Minimum (Position A)	-77,31	-77,31	0,0%	-512,196	-458,56	11,70%
N-S Cycles	Maximum (Position D)	91,6508	90,64	1,12%	365,317	361,85	0,96%
	Minimum (Position C)	-77,313	-76,37	1,23%	-517,626	-431,7	19,90%
Diagonal Cycles E-F	Maximum (Position F)	74,99	74,39	0,81%	552,22	459,56	20,16%
	Minimum (Position E)	-77,25	-77,01	0,31%	-663,91	-428,22	55,04%

Table 5.2 Comparison Between Numerical and Experimental Results TUB

One of drawbacks of using the MVLEM-3D element was the inability to spot damage mechanisms such as crushing of concrete (TUB) and fracture of steel bars (TUA) which was clear in the strength loss in the force deformation of the experimental results.

5.2. TUC

TUC was mainly loaded in the diagonal directions, the accuracy of the model to represent the lateral load carrying capacity was very similar to that of the diagonal cycles in TUA and TUB. For the diagonal loading an increase in predicting the capacity of the wall ranging between 20-40% for varying loading positions with a maximum error recorded at position E. This error was mainly because of the plane section assumption of the MVLEM-3D formulation the same reason mentioned for TUA and TUB in diagonal directions.

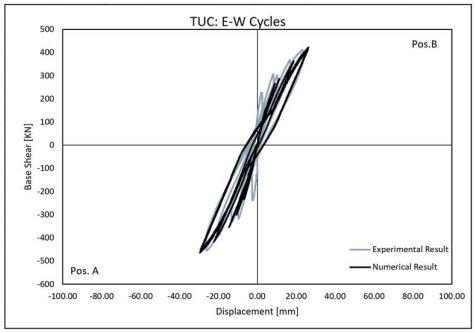

(a) E-W Direction-TUC

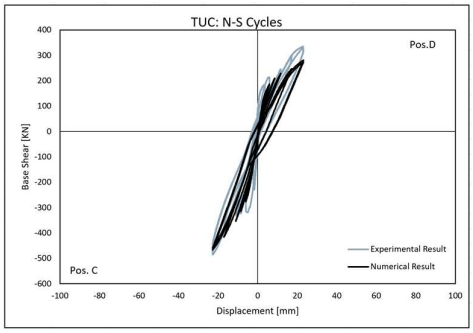

(b) N-S Direction-TUC

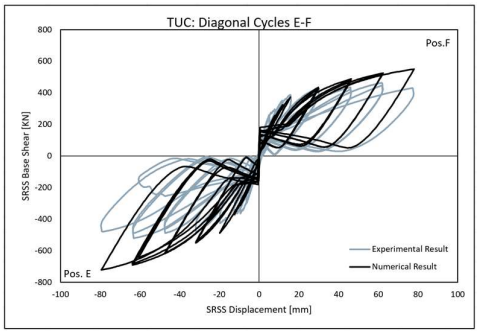

(c) Diagonal Direction E-F-TUC

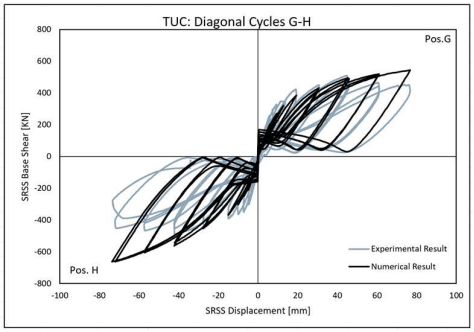

(d) Diagonal Direction G-H-TUC

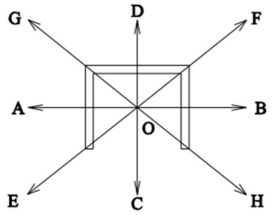

(f) Loading Direction-TUC

Figure 5.3 Comparison of Experimental and Numerical Force-Deformation Relationship for TUC

Experimental Result

Numerical Result

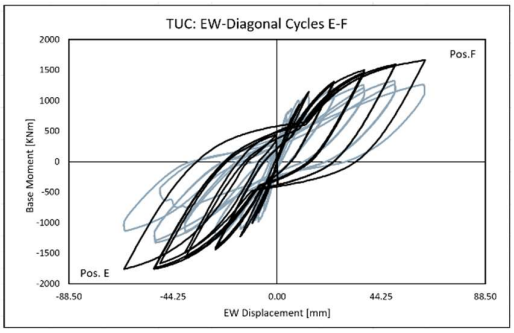

(a) E-W Diagonal cycle position E-F for TUC

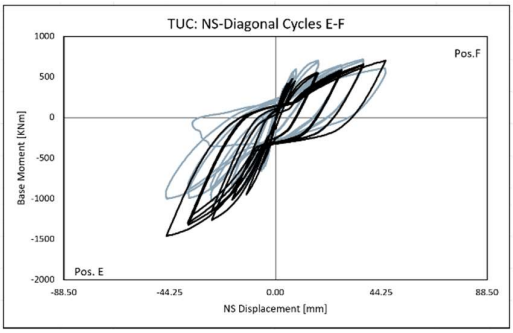

(b) N-S Diagonal cycle position E-F for TUC

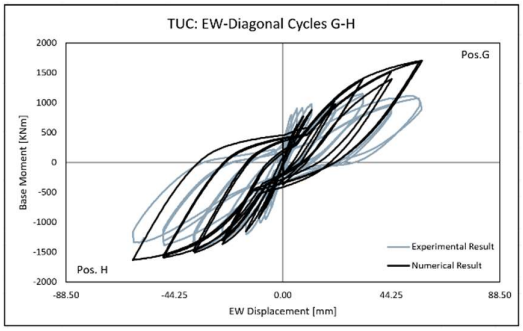

(c) E-W Diagonal cycle position G-H for TUC

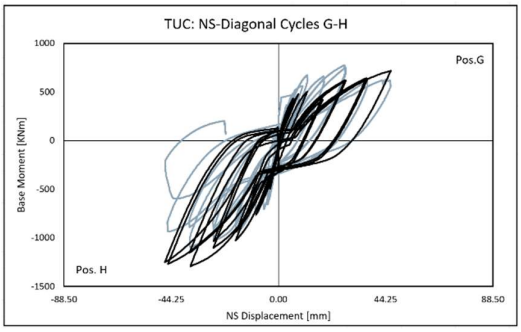

(d) N-S Diagonal cycle position G-H for TUC

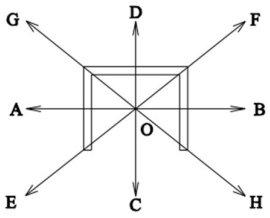

(f) Loading Direction-TUC

Figure 5.4 Comparison of Experimental and Numerical Force-Deformation Relationship for diagonal cycle for TUC

Experimental Result

Numerical Result

For the overall shape of the hysteresis loops, similar to TUA and TUB the numerical initial loading stiffness and the overall shape of the loop were in good agreement with the experimental features. The strength loss from the out-of-plane instability and compression failure of the flange was not represented in the model which was shown by a significant drop in the load-deformation relationship of the experimental results.

Detailed calculations of the accuracy of the imposed displacements and the response in terms of base shear are shown in Table 5.1, Table 5.2 and Table 5.3 for the diagonal cycles, the base shear was calculated based on SRSS combination.

TUC		Imposed Displacement [mm]			Base Shear [KN]		
		Numerical Result	Experimental Result	Error	Numerical Result	Experimental Result	Error
Diagonal Cycles E-F	Maximum (Position F)	78,04	77,86	0,23%	550,55	464,11	18,62%
	Minimum (Position E)	-79,43	-79,66	0,28%	-721,92	-520,04	38,82%
Diagonal Cycles G-H	Maximum (Position G)	76,77	76,73	0,06%	544,29	510,13	6,70%
	Minimum (Position H)	-73,66	-73,44	0,30%	-662,23	-490,08	35,13%

Table 5.3 Comparison Between Numerical and Experimental Results TUC

For the studying of the effect of the plane section hypothesis on the results, the next figures show the strain distribution on the base of the wall above the foundation for different loading positions (Figure 5.5- Figure 5.7). It was observed from the analytical results that when loading in the N-S direction (Position C), the compressive and tensile strains are well predicted in comparison to the experimental strain distribution. Moreover, the length of the compressive zone (neutral axis depth) is also in good agreement with the experimental data.

By studying the diagonal direction, the experimental data shows that the plane section assumption does not hold as the strain distribution becomes highly non-linear at the base of the test unit. This is a limit for the MVLEM-3D element as it is implemented based on the plane section assumption. Nevertheless, at drift levels less than the yield limit around 0.4% where the response was still in the elastic zone the numerical results give a good approximation for the strain distribution at the base. Despite that, when reaching higher drift levels at 1% drift post yielding, the plane section assumption implemented in the MVLEM-3D fails to represent correctly the compressive and tensile zone at the test units' corners. Diagonal loading in the direction of the tips of the flanges, shows an overestimation of the strain distribution of 20-30% at the corners of the wall, while loading in the direction of the wall corners the element overestimates the tensile strains along the flanges and the corner on tension by 40-50% and undervalue the compressive strains in the corner subjected to compression (in the direction of the loading). All the inaccuracies of predicting the value and the length (neutral axis depth) of the compressive and tensile strains led to an overestimation of the overall lateral load capacity of the test units.

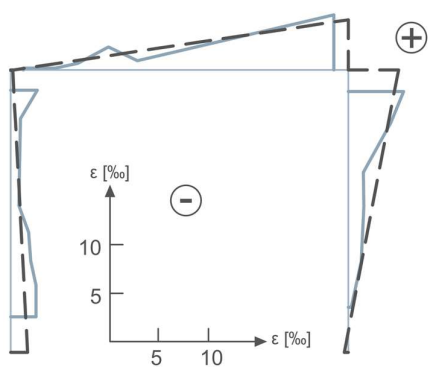

(a) Position E

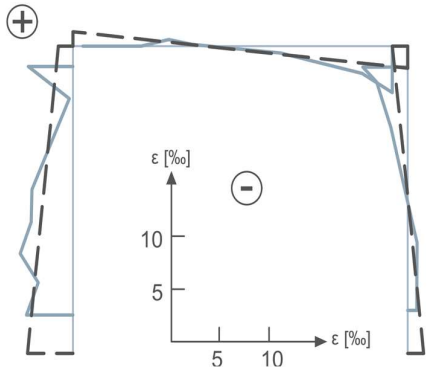

(b) Position F

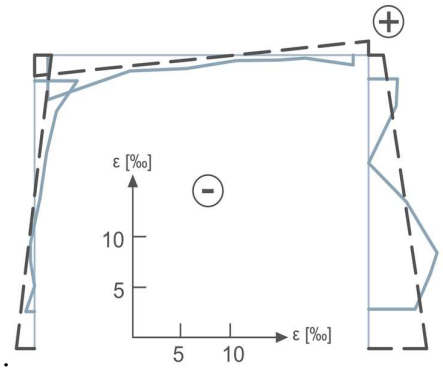

(c) Position G

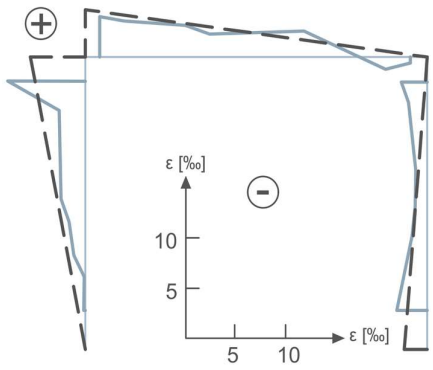

(d) Position H

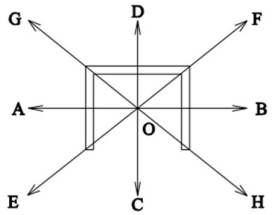

(f) loading directions

Figure 5.5 Strains at the Base of TUC at 0.4% drift

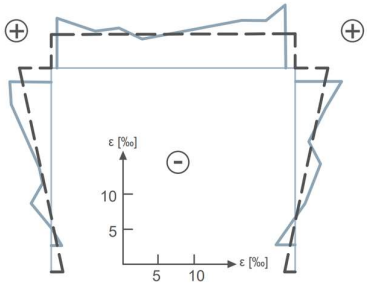

Figure 5.6 Strains at the Base of TUC at 0.4% drift at position C

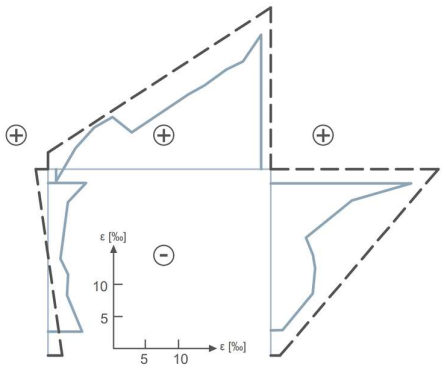

(a) Position E

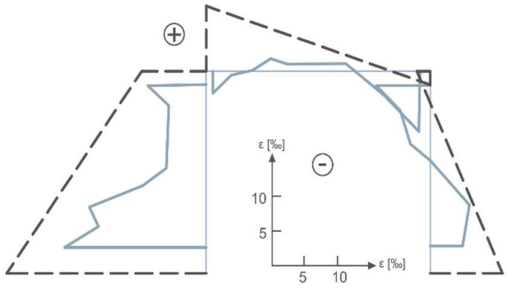

(b) Position F

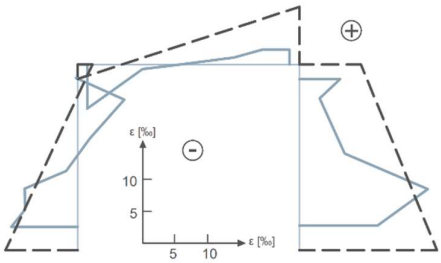

(c) Position G

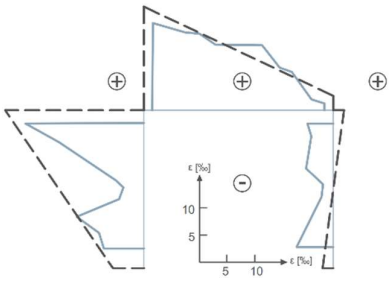

(d) Position H

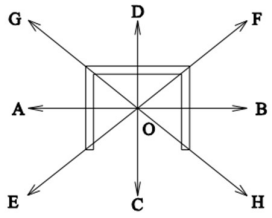

(e) loading directions

Figure 5.7 Strains at the Base of TUC at 1% drift

6 Conclusion and Future Work

6.1. Summary and Conclusion

The main objective of this thesis is to represent the peculiarities of the behavior of non-planar walls subjected to bi-directional loading and developing a numerical model that could be used to predict the behavior of non-planar walls. Firstly, it started by deeply understanding the behavior of walls tested under different loading protocols and different geometry aspects in order to highlight the effective parameters in the behavior of the non-planar walls. Then, three experimental U-shaped test units were chosen to further study their setting up during the test and study their failure mechanisms. Furthermore, Numerical models were built up for these test units by OpenSees which used the MVLEM 3-D element to simulate a behavior which is similar to the behavior of the test units under experimental testing by calibrating the material models for steel, unconfined concrete and confined concrete. Further, verification of the numerical results was made to make sure that the behavior of the walls was well captured. Some Major conclusions are noted in the following points:

(A) The plane section assumption that is considered in the formulation of MVLEM 3-D overestimates the lateral load capacity in the diagonal directions. While the plane section assumption is still valid for estimating the capacity of the walls in their principal directions (i.e., E-W, N-S directions).

(B) Flanges of the non-planar walls are likely to be subjected to out-of-plane buckling when subjected to bi-directional loading. While for the planar walls, they are exposed to in-plane and out-of-plane instability that results from the imperfections during construction phase.

(C) For flanges of the non-planar wall that are subjected to diagonal loading, in case one flange tip to be compressed, this loading direction shows a bigger compression depth of the flange , which will demand a higher confinement lengths with respect to any other loading direction. So, it is recommended to better consider the confinement length of the boundary elements of the flanges based on the diagonal loading not only the principal loading directions.

(D) Some observed failure mechanisms (i.e., out of plane buckling of the wall, rupture of the reinforcement bars and crushing of concrete) were not captured in the numerical results, which is a major limitation of using the modeling technique that was followed.

6.2. Future Work

While designing non-planar composite walls, most Engineers fail to consider the diagonal direction and consider only the principal directions. In fact, most of the analysis softwares only consider the behavior in the principal directions and neglects the diagonal direction. Hence, a primary goal in the future scope of work is to develop uncomplicated analysis procedures that would consider correctly the carrying capacity (i.e., in terms of moment and displacement) of the non-planar walls. Furthermore, more research could be done in developing new material models and modeling elements that would overcome the limitations of the current ones such as inability to capture experimental failure mechanisms and elements using only the plane section hypothesis.

Bibliography

ACI 318-05. (2005). *Consulting Members BUILDING CODE REQUIREMENTS FOR STRUCTURAL CONCRETE (ACI 318-05) AND COMMENTARY (ACI 318R-05) REPORTED BY ACI COMMITTEE 318 ACI Committee 318 Structural Building Code † Deceased*.

Akelyan, S., & Brandow, G. (2020). *2020 LATBSDC Alternative Analysis and Design Procedure 1*.

Arabzadeh, H., Goguen, K., Pelletier, K., Bouaanani, N., Galal, K., & Léger, P. (2017). *EVALUATION OF FINITE AND FIBER ELEMENTS RC MODELS FOR NONLINEAR CYCLIC ANALYSIS OF U SHAPED SHEAR WALL*.

ASCE-7. (2006). *ASCE 7:05 Minimum design loads for buildings and other structures*. American Society of Civil Engineers/Structural Engineering Institute.

Belarbi, A., & Hsu, TC. (1994). Constitutive laws of concrete in tension and reinforcing bars stiffened by concrete. *ACI Structural Journal*, 465–474.

Beyer, K., Dazio, A., & Priestley, M. J. N. (2008a). Inelastic wide-column models for U-shaped reinforced concrete walls. *Journal of Earthquake Engineering*, *12*(SUPPL. 1), 1–33. https://doi.org/10.1080/13632460801922571

Beyer, K., Dazio, A., & Priestley, M. J. N. (2008b). Quasi-static cyclic tests of two U-shaped reinforced concrete walls. *Journal of Earthquake Engineering*, *12*(7), 1023–1053. https://doi.org/10.1080/13632460802003272

Beyer, K., Dazio, A., & Priestley, M. J. N. (2011). *Shear Deformations of Slender Reinforced Concrete Walls under Seismic Loading ACI Structural Journal*. https://www.researchgate.net/publication/286384751

Brueggen, B. L., & French, C. E. (2009). *Performance of T-shaped Reinforced Concrete Structural Walls under Multi-Directional Loading* [PhD Dissertation]. University of Minnesota.

Calabrese, A., Almeida, J. P., & Pinho, R. (2010). Numerical issues in distributed inelasticity modeling of RC frame elements for seismic analysis. *Journal of Earthquake Engineering*, *14*(SUPPL. 1), 38–68. https://doi.org/10.1080/13632461003651869

Constantin, Raluca., & Beyer, Katrin. (2016). Behaviour of U-shaped RC walls under quasi-static cyclic diagonal loading. *Engineering Structures*, *106*, 36–52. https://doi.org/10.1016/j.engstruct.2015.10.018

Correia, A. A., Almeida, J. P., & Pinho, R. (2015). Force-based higher-order beam element with flexural-shear-torsional interaction in 3D frames. Part I: Theory. *Engineering Structures*, *89*, 204–217. https://doi.org/10.1016/j.engstruct.2014.10.024

EN 1998-1. (1998). *EN 1998-1: Eurocode 8: Design of structures for earthquake resistance – Part 1: General rules, seismic actions and rules for buildings*.

Fllippou, F. E., Popov, E. P., & Bertero, V. V. (1983). *EFFECTS OF BOND DETERIORATION ON HYSTERETIC BEHAVIOR OF REINFORCED CONCRETE JOINTS by NATIONAL TECHNICAL INFORMATION SERVICE*.

Gogus Arup, A. (2010). *Structural Wall Systems-Nonlinear Modeling and Collapse Assessment of Shear Walls and Slab-Column Frames*. https://www.researchgate.net/publication/272089615

Hines, E. M., Dazio, A., & Seible, F. (2006). Structural Testing of New East Bay Skyway Piers. *ACI Structural Journal*.

Ile, N., & Reynouard, J. M. (2005). Behaviour of U-shaped walls subjected to uniaxial and biaxial cyclic lateral loading. *Journal of Earthquake Engineering*, *9*(1), 67–94. https://doi.org/10.1080/13632460509350534

Inada, K., Chosa, K., Sato, H., Kono, S., & Watanabe, F. (2008, October 12). SEISMIC PERFORMANCE OF RC L-SHAPED CORE STRUCTURAL WALLS. *Proceeding of the 14th World Conference on Earthquake Engineering* .

Kent, DC., & Park, R. (1971). Flexural members with confined concrete. *Journal of the Structural Division* .

Kolozvari, K., Kalbasi, K., Orakcal, K., & Wallace, J. (2021). Three-dimensional model for nonlinear analysis of slender flanged reinforced concrete walls. *Engineering Structures*, *236*. https://doi.org/10.1016/j.engstruct.2021.112105

Kolozvari, K., Orackcal, K., & Wallace, J. (2016). *Displacement-based Beam-Column element. OpenSees Wiki.* Https://Opensees.Berke Ley.Edu/Wiki/Index.Php/Displacement-Based_Beam-Column_Element.

Kolozvari, K., Orakcal, K., & Wallace, J. W. (2018). New opensees models for simulating nonlinear flexural and coupled shear-flexural behavior of RC walls and columns. *Computers and Structures*, *196*, 246–262. https://doi.org/10.1016/j.compstruc.2017.10.010

Kolozvari, K., & Wallace, J. W. (2016). Practical Nonlinear Modeling of Reinforced Concrete Structural Walls. *Journal of Structural Engineering*, *142*(12). https://doi.org/10.1061/(asce)st.1943-541x.0001492

Li, W., & Li, Q. N. (2012). Seismic performance of l-shaped rc shear wall subjected to cyclic loading. *Structural Design of Tall and Special Buildings*, *21*(12), 855–866. https://doi.org/10.1002/tal.645

Lowes, L., Behrouzi, A., Mock, A., Lehman, D., & Kuchma, D. (2014). Large Scale Testing of C-Shaped Reinforced Concrete Walls. *A Report to the Chares Pankow Foundation on Grant*.

Mander, J. B., Priestley, M. J. N., & Park, R. (1988). THEORETICAL STRESS-STRAIN MODEL FOR CONFINED CONCRETE. *Journal of Structural Engineering*, 1804–1826.

Mazzoni, S., Mckenna, F., Scott, M. H., Fenves, G. L., & Iii, A. (2006). *Open System for Earthquake Engineering Simulation (OpenSees) OpenSees Command Language Manual*.

Menegotto, M., & Pinto, E. (1973). *Method of analysis for cyclically loaded R.C. plane frames including changes in geometry and non-elastic behaviour of elements under combined normal force and bending*. https://doi.org/10.5169/seals-13741

Oesterle, RG., Aristizabal-Ochoa, JD., Fiorato, AE., Russel, HG., & Corely, WG. (1979). *"Earthquake Resistant Structural Walls - Tests of Isolated Walls - Phase II" Report to the National Science Foundation for Grant No. ENV77-15333*.

Oesterle, RG., Fiorato, AE., Johal, LS., Carpenter, JE., Russel, HG., & Corely, WG. (1976). *"Earthquake Resistant Structural Walls - Tests of Isolated Walls" Report to the National Science Foundation for Grant No. GI-43880*.

Orackal, K., Wallace, J., & Conte, P. (2004). Flexural Modeling of Reinforced Concrete Walls— Model Attributes. *ACI Structural Journal*.

PEER. (2017). *TBI Tall Buildings Initiative Guidelines for Performance-Based Seismic Design of Tall Buildings*.

Pégon, P., Plumier, C., Pinto, A., Molina, J., Gonzalez, P., Gonzalez, P., & Hubert, O. (2000). U-shaped walls: description of the experimental set-up. *TMR-ICONS-TOPIC5, JRC Ispra*, 23.

Reynouard, J. M., & Fardis, M. N. (2001). *"Shear wall structures," Cafeel-Ecoest Thematic Report No. 5*.

Saatcioglu, M., & Razvi, S. R. (1992). Strength and Ductility of Confined Concrete. *Journal of Structural Engineering*, *118*(6), 1590–1607. https://doi.org/10.1061/(asce)0733-9445(1992)118:6(1590)

Scott, BD., Park, R., & Priestley, MJN. (1982). Stress-Strain Behavior of Concrete Confined Overlapping Hoops at Low and High Strain Rates. *ACI Journal*.

Thomsen, J. H., & Wallace, J. W. (2004). Displacement-Based Design of Slender Reinforced Concrete Structural Walls-Experimental Verification. *JOURNAL OF STRUCTURAL ENGINEERING*, 618–630. https://doi.org/10.1061/ASCE0733-94452004130:4618

Vulcano A. (1992). *NONLINEAR SEISMIC ANALYSIS AND DESIGN OF REINFORCED CONCRETE BUILDINGS* (Krawinkler H & Fajfar P, Eds.). Elsevier Science.

Wallace, J. W., & Moehle, J. P. (1992). Ductility and Detailing Requirements of Bearing Wall Buildings. *Journal of Structural Engineering*, *118*(6), 1625–1644. https://doi.org/10.1061/(asce)0733-9445(1992)118:6(1625)

Yassin, MH. (1994). *Nonlinear analysis of prestressed concrete structures under monotonic and cyclic loads* [PhD dissertation]. University of California.

Appendix

Here you can find the STKO files and Input files for all the models created in this thesis.

https://polimi365-my.sharepoint.com/personal/10816970_polimi_it/_layouts/15/onedrive.aspx?id=%2Fpersonal%2F10816970%5Fpolimi%5Fit%2FDocuments%2FInput%20Files&view=0